



# Spatial variation, multi-meteorological factors and potential source analysis of air pollutants in Chengdu megacity of Chengdu-Chongqing economic circle

Xiaoju Li<sup>1,2</sup> · Luqman Chuah Abdullah<sup>2,3</sup> · Jinzhao Hu<sup>1</sup> · Shafreeza Sobri<sup>2</sup> · Mohamad Syazarudin Md Said<sup>2</sup> · Siti Aslina Hussain<sup>2</sup> · Tan Poh Aun<sup>4</sup>

Received: 27 February 2024 / Accepted: 8 August 2024  
© The Author(s), under exclusive licence to Springer Nature B.V. 2024

## Abstract

Affected by unique topography, meteorological factors and high emission sources, it is crucial to have an in-depth understanding of the air pollution characteristics of Chengdu megacity. This research investigated the spatial evolution features of the six criteria pollutants in Chengdu from 2014 to 2020. The relationship between air pollutants and multi-meteorological factors also will be systematically elucidated. Together with the backward trajectory model, the potential source areas of PM<sub>2.5</sub> and O<sub>3</sub> were further simulated. The results revealed that there is spatial heterogeneity in the distribution of air pollution in Chengdu. Besides, the concentrations of PM<sub>2.5</sub>, PM<sub>10</sub>, SO<sub>2</sub>, NO<sub>2</sub> and CO are only positively correlated with pressure. While, O<sub>3</sub> only shows a negative correlation with relative humidity and pressure. Furthermore, regional transport is also one of the important contributing sources of PM<sub>2.5</sub> and O<sub>3</sub>. This study can accurately grasp the status of regional air pollution, and provide accurate and feasible solutions for the collaborative reduction of air pollution in the Cheng-Yu area. Furthermore, it provides data references for exploring efficient air pollution control measures in complex terrain, and also accumulates some experience for the megacities of similar situations in the world.

**Keywords** Atmospheric pollutant · Cheng-Yu Economic Circle · Spatial Heterogeneity · Multi-meteorological parameters · Potential sources identification · Synergic control

## Highlights:

- Spatial heterogeneity can be observed in the distribution of pollutants.
- Pollutants are affected by multi-meteorological factors and exist seasonal differences.
- Potential source regions of PM<sub>2.5</sub> and O<sub>3</sub> were quantitatively simulated.
- Promote the synergistic effect of pollution and carbon reduction.

✉ Luqman Chuah Abdullah  
chuah@upm.edu.my

- <sup>1</sup> Xichang University, No. 1 Xuefu Road, Anning Town, Xichang City 615000, Sichuan Province, China
- <sup>2</sup> Department of Chemical and Environmental Engineering, Faculty of Engineering, University Putra Malaysia, 43400 UPM Serdang, Selangor, Malaysia
- <sup>3</sup> Institute of Tropical Forestry and Forest Products, Universiti Putra Malaysia, 43400 UPM Serdang, Selangor, Malaysia
- <sup>4</sup> SOx NOx Asia Sdn Bhd, UEP Subang Jaya Selangor Darul Ehsan, 47620 Subang Jaya, Malaysia

## Introduction

The world is currently facing the double burden of climate change and air pollution. Studies have proven that air pollution is one of the key causes of global and regional climate crisis, threatening the sustainable development of socio-economic, human well-being and accelerating the pandemic with complex mechanisms (Fig. 1) (Åström, 2023; Liang et al. 2023a, b; Lei et al., 2022). The process of industrialization and urbanization has promoted a sharp increase in fossil energy consumption and aggravated global air pollution (Fig. S1). Around 4.2 million premature deaths worldwide are caused by air pollution each year (Gonzalez et al. 2022). Currently, China's air pollution presents the characteristics of multiple pollution sources, superposition of multiple pollutants, and combination of urban and regional pollution (Table 1). Moreover, the top three CO<sub>2</sub> emissions in 2020 are China, the United States and India, accounting for 30.93%, 13.86% and 7.19% of the global total carbon dioxide emissions respectively (Fig. S2). Coordinated

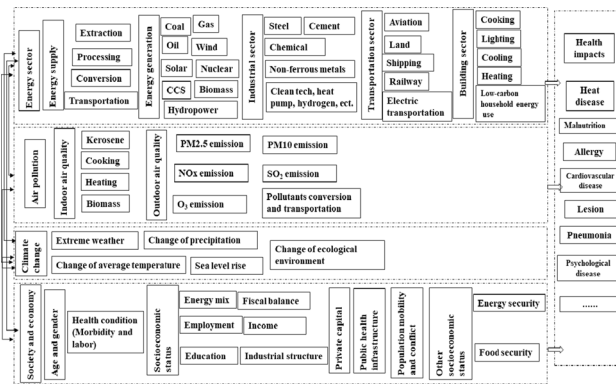


**Fig. 1** Links between air pollution, energy, climate and health

reduction of pollutants and carbon emissions is the fundamental guarantee for China to reach carbon neutrality by 2060 (Dong et al. 2022; Li et al. 2023). In 2020, the proportion of severe and above pollution day (1.2%) has improved significantly compared to 2015 (2.8%) (Azmi et al. 2023; Zhang et al. 2022a, b, c). However, the concentration of  $PM_{2.5}$  improves slowly, and the reduction of  $NO_x$  emission is not significant. Moreover,  $O_3$  pollution is becoming more and more prominent, and the coordinated reduction of  $PM_{2.5}$  and  $O_3$  has become a severe challenge.

The regions with the worst air pollution in China are mainly concentrated in the Beijing-Tianjin-Hebei region (BTH), the Pearl River Delta (PRD), the Yangtze River Delta (YRD), the Fenwei Plain (FWP), Jingjinji (JJJ) and the Sichuan basin (SCB) (Fig. 2) (Feng et al. 2023). Since the location of the SCB is unique worldwide, it provides an excellent platform for complex terrain air pollution investigations. However, unlike other heavily polluted regions, air pollution in the SCB is not well understood. Based on the relevant regulations of the Emergency Plan for Heavy Pollution Weather in Sichuan Province (revised in 2018), with eight or more cities reaching moderate and above levels of pollution as the standard, it was found that there were 21 regional air pollution processes in SCB during 2015–2018 (Table S1). Relevant literature has confirmed that severe air pollution frequently occurs in highly industrialized and urbanized cities with complex terrains, such as Beijing, Lanzhou and Chengdu in China (Fan et al. 2019; Meng et al., 2020)<sup>1</sup>.

<sup>1</sup> PSCF: Potential Source Contribution Function; CWT: Concentration Weighted Trajectory; IEA: International Energy Agency; BTH: Beijing-Tianjin-Hebei region; YRD: Yangtze River Delta; PRD: Pearl River Delta; FWP: Fenwei Plain; JJJ: Jingjinji; SCB: Sichuan Basin; VOCs: Volatile Organic Compounds; WHO, 2021AQGs: World Health Organization, Global Air Quality Guidelines; TEM: Temperature; PRS: Pressure; RHU: Relative Humidity; PRE: Precipitation; GST: Ground Surface Temperature; SSD: Sunshine Duration; WPSCF: Weighted Potential Source Contribution Function; WCWT: Weighted Concentration Weighted Trajectory.

As a megacity, Chengdu has a more arduous task of preventing ecological and environmental risks, and the establishment of a long-term mechanism for normalized collaborative governance still faces challenges (Fan et al. 2019). Although numerous research have been done in different regions of SCB in recent years, it is still lack of detailed and in-depth studies on Chengdu (Hou et al. 2022; Hu and Wang 2021; Tan et al. 2023). Moreover, most of the reported studies explore the short-term impacts and typical pollution events, and are limited to the data of a single pollutant at a few sites. Only few studies have explored the spatial variation characteristics of pollutants at multiple sites over a long period of time. Therefore, the results obtained by these studies may not conclusive and could lack of spatial contrast. Nevertheless, there is a lack of detailed discussion of the variation characteristics of multiple meteorological parameters at multiple stations and their impact mechanisms with multiple pollutants in previous studies. In addition, the trajectory clustering model, Potential Source Contribution Function (PSCF) model and Concentration Weighted Trajectory (CWT) models are effective tools for exploring regional pollution transport (Berriban et al. 2022; Cao et al. 2023), but they are rarely used in SCB regions, especially in the Chengdu megacity. Extensive research has revealed that even for the same research subjects, there may be significant bias in the results due to differences in research parameters and methods (Liu et al. 2021). Therefore, it is difficult for some existing studies to accurately characterize the long-term pollution status of Chengdu megacity.

Through the different research methods and models, a more detailed analysis of air pollution in megacities from the perspectives of spatial distribution, meteorological influence factors, and regional transmission can accurately grasp the status of regional air pollution, and provide reference for traceability of pollution sources and more accurate trend prediction. Besides, this research can provide new methods and data references for exploring efficient air pollution control measures in complex topography, and also accumulate some experience in the regional joint prevention of megacities in similar situations in the world. Using the long-term monitoring data pollutants in Chengdu from 2014 to 2020, the spatial fluctuation characteristics of the six criteria pollutants ( $PM_{2.5}$ ,  $PM_{10}$ ,  $NO_2$ ,  $SO_2$ ,  $O_3$  and CO) were comprehensively investigated. The annual, seasonal and monthly spatiotemporal evolution of seven meteorological factors was then systematically elucidated. Furthermore, a comprehensive and detailed analysis of the effects of multi-meteorological parameters on the air pollutants also were explored. Finally, combined with the cluster analysis, PSCF model and the CWT method, the potential source areas of  $PM_{2.5}$  and  $O_3$  in 2020 were further quantitatively simulated from different season.

**Table 1** Evolution of air pollution in China

	1980–1990	1990–2000	2000–	Ref
Main source of pollution	Coal burning, industrial	Coal burning, industry, dust	Coal combustion, industry, motor vehicles, dust	(Song et al. 2022a, b; Xu et al. 2020; Zhang et al. 2017)
Main pollutants	SO <sub>2</sub> , Total solid particles, PM <sub>10</sub>	SO <sub>2</sub> , TSP, NO <sub>x</sub> , PM <sub>10</sub>	SO <sub>2</sub> , PM <sub>10</sub> , PM <sub>2.5</sub> , NO <sub>x</sub> , VOCs, NH <sub>3</sub> , CO, O <sub>3</sub>	
Major air pollution issues	Coal burning	Coal burning, particulate matter and acid rain	Coal burning, haze, acid rain, photochemical pollution, toxic and harmful substances	
Air pollution scale	local	local + regional	Local + Regional + Global	

## Methodology

### Study area

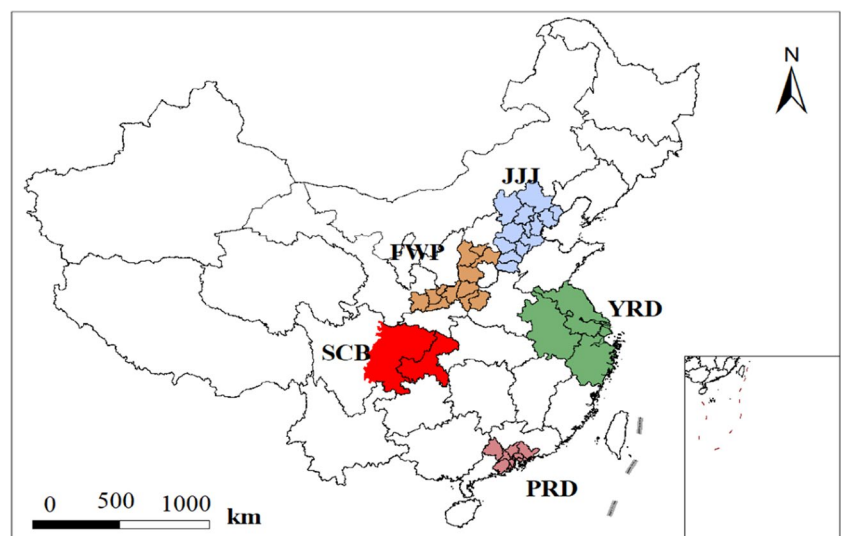
Surrounded by mountains, the Chengdu megacity (30° 05' N-31° 26' N, 102° 54' E-104° 53' E) is located on the western edge of the SCB, with a total area of 14,605 km<sup>2</sup> (larger than Shanghai, Tianjin megacities) (Chen et al. 2022a, b, c; Deng et al. 2019) (Fig. 3a). Compared with 2010, in 2020, its GDP, urbanization rate, population and car ownership have increased by 200%, 19.8%, 49.04% and 200%, respectively (Fig. 4). By the end of 2021, the resident population had reached 21.19 million, the urbanization rate had reached about 79.5%, the total value of regional power generation was 1.99 billion and the number of motor vehicles was about 6.26 million (National Bureau of Statistics of China 2022). The industry is mainly characterized by automobiles, coal-fired power plants, building materials, machinery, food, etc. (Zhang et al. 2018; Wang et al. 2018a, b). In addition, the terrain of this area is of high in the west and low in the east, with a height difference of 4,966 m, and the terrain is relatively closed (Ning

et al. 2019; Yang et al. 2020). The altitude in this area is averagely 750 m, with the lowest altitude of 359 m. Due to the huge vertical height difference, unique landform types of plains (40.1%), hills (27.6%) and mountains (32.3%) are formed in this area.

### Data collection

The six criteria pollutants in this study are mainly based on the data from eight state-controlled monitoring stations in Chengdu (Fig. 3b). Besides, seven surface meteorological parameters (Win, Temperature (TEM), Ground Surface Temperature (GST), Relative Humidity (RHU), Precipitation (PRE), Pressure (PRS), Sunshine Duration (SSD)) mainly come from 13 meteorological stations (Fig. 3b). Besides, the analysis data also refers to third-party sources, such as China air quality platform (<http://www.aqistudy.cn/>). Daily meteorological data mainly refer Chengdu Meteorological Monitoring Database (<http://data.cma.cn/>). Besides, the Geospatial Data Cloud (<https://www.gscloud.cn/>), Sichuan and Chengdu Statistical Yearbook (<http://m.chdstats.gov.cn/>) also referred

**Fig. 2** The locations of the five urban agglomerations in China



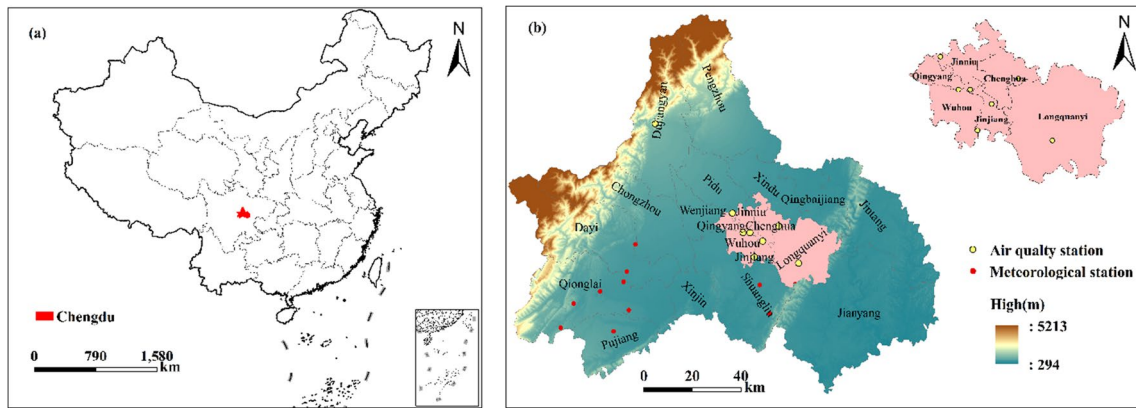


Fig. 3 (a) The location of Chengdu and (b) the topography and monitoring station of Chengdu

to obtaining geographic information data and socio-economic data. Also, meteorological data obtained from the National Center for Environmental Prediction of the United States (<ftp://arlftp.arlhq.noaa.gov/pub>) are used for backward trajectory model. In addition, the parameter settings in the backward trajectory model are shown in Table 2 (Bai et al. 2021a, b; Berriban et al. 2022).

**Analysis methods**

**Correlation analysis** As a non-parametric test method, the Spearman rank correlation coefficient is mainly used to present the relationship between variables (Gao et al. 2016; Tarasov et al. 2018). When there is no repeated data and one variable is a strictly monotonic function of another variable, the Spearman rank correlation coefficient is equal to +1 or -1, which is called the complete Spearman rank correlation of variables (Liu et al. 2023; Qi et al. 2023; Xu et al. 2022). When all rank values are integers, the rank correlation coefficient can be calculated by the formula Eq. 1.

$$r_s = 1 - \frac{6 \sum d_i^2}{n(n^2 - 1)} \tag{1}$$

$d_i$  is the rank difference between the two variables in each set of observations,  $n$  is the total number of paired samples. This study uses Spearman’s correlation analysis to clarify the relationship between meteorological indicators and air pollutant indicators in order to understand the strength of the correlation between variables and focus on controlling pollutants that have a greater impact on air quality.

**Interpolation techniques** Spatial interpolation is a method of converting discrete point measurement data into a continuous data surface and comparing it with other spatial distribution patterns. The most commonly used methods of spatial interpolation include Inverse Distance Weighting (IDW) interpolation, Kriging interpolation, Spline function method, etc. (Kumar et al. 2020; Lofata 2022; Pinto et al. 2020). Among them, Kriging is a prominent interpolation technique and the most commonly used spatial interpolation algorithm. Kriging interpolation is more accurate than other interpolation methods. By considering spatial autocorrelation and the weight of data points, this method can generate a more accurate spatial prediction model. In addition, this method not only considers the numerical value of the data point, but also the spatial correlation of the variable. Finally, Kriging interpolation can select different variogram models according to different data distribution and autocorrelation patterns, which is highly

Fig. 4 Area and population and GDP in division of Chengdu in 2020 ( Tan et al. 2023; Zhang et al. 2022a, b, c; Zhu et al. 2020)

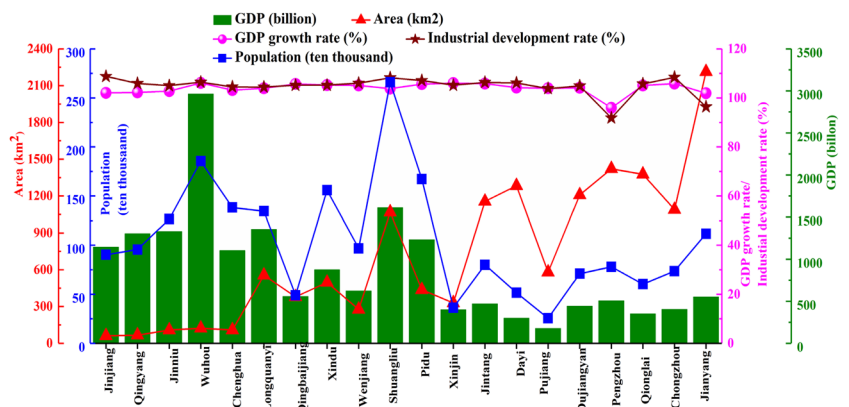


**Table 2** 2014–2020 backward trajectory model parameters

Parameter	Parameter settings
Direction of trajectory	Backward
Trajectory running time	24 h
Trajectory interval time	1 h
Height	500mAGL
Threshold value of PM <sub>2.5</sub> pollution day	75 μg/m <sup>3</sup>
Threshold value of O <sub>3</sub> pollution day	160 μg/m <sup>3</sup>

flexible (Shukla et al. 2020; Yang & Hu 2018). Kriging is a geo-statistical technique that is an interpolation method for unbiased optimal estimation of variables within a limited area (hukla et al., 2020; Yang & Hu 2018). In the kriging method, it is assumed that the joint probability distribution of the entire research space is stationary, and uniform in all directions. In this method, (x, y) set as the coordinates of a certain space data point and z(x, y) represents its value. For z<sub>0</sub> = z(x<sub>0</sub>, y<sub>0</sub>), the Kriging interpolation formula is shown in (Eq. 2) (Beauchamp et al. 2018; Kumar et al. 2022; Lotfata 2022).

$$\hat{z}_0 = \sum_{i=1}^n w_i z_i \tag{2}$$

Since the Kriging method is unbiased and has the smallest variance, the undetermined weight coefficient w<sub>i</sub> (i = 1, 2, ..., n) of the unbiased condition satisfies the relational expression (Eq. 3):

$$\sum_{i=1}^n W_i = 1 \tag{3}$$

When there is no bias and the kriging variance is the smallest, the variance group of undetermined weight coefficients w<sub>i</sub> can be obtained (Eq. 4).  $\hat{z}_0$  represents the estimation value at the point (x<sub>0</sub>, y<sub>0</sub>), z<sub>i</sub> (1 ≤ i ≤ n) represents the observation value of n points near of the (x<sub>0</sub>, y<sub>0</sub>), w<sub>i</sub> represents the weight coefficient of the observation value z<sub>i</sub> (1 ≤ i ≤ n) and the relative point (x<sub>0</sub>, y<sub>0</sub>). C(x<sub>i</sub>, y<sub>i</sub>) is the covariance function of z<sub>i</sub> and z<sub>j</sub>.

$$\begin{cases} \sum_{i=1}^n w_i C(x_i, x_j) + \mu = C(x_0, x_j), (j = 1, 2, \dots, n) \\ \sum_{i=1}^n w_i = 1 \end{cases} \tag{4}$$

**Backward trajectory clustering** Due to the spatial similarity of air mass trajectories, the backward trajectory clustering method can group all trajectories and calculate the spatial dissimilarity (SPVAR) and total spatial difference (TSV) of each trajectory from the clustered average trajectory (Foy et al. 2021; Li et al. 2017a, b). Then, according to the relationship between TSV and n, the number of clusters is judged, and air mass trajectories reaching at the receiving

point of the model are grouped and clustered (Sasmita et al. 2022). The SPVAR of each cluster is expressed as Eq 0.5:

$$SPVAR = \sum_{i=1}^x D_i \tag{5}$$

Trajectory clustering is mainly calculated by two clustering methods, angular distance and Euclidean distance (Cao et al. 2020). This study adopts the Euclidean distance method, and the principle of grouping and clustering is to make the difference in moving speed and direction between the trajectories in the group extremely small, and at the same time, the difference between groups is maximized. The Euclidean distance between two trajectories within a particular cluster is defined as Eq 0.6 (Li et al. 2017a, b; Sen et al. 2017). X<sub>1</sub>(Y<sub>1</sub>) and X<sub>2</sub>(Y<sub>2</sub>) is the trajectory 1 and 2.

$$d_{12} = \sqrt{((X_1(i) - X_2(i))^2 + (Y_1(i) - Y_2(i))^2)} \tag{6}$$

**PSCF model** The proportion of pollution trajectories and the distribution of potential contributing source areas of grid cells to high pollutant loads at receptor sites can be found through PSCF values. The high value area of PSCF is the main area of high pollutant concentration (Stojić & Stanišić, 2017). In PSCF model, Chengdu (30.66°N, 104.10°E) was set as the starting point and the simulation start altitude is set to 500 m (Deng et al. 2020; Kaskaoutis et al. 2019). The thresholds of PM<sub>2.5</sub> and O<sub>3</sub> in the model are set at 75 μg/m<sup>3</sup> and 160 μg/m<sup>3</sup>, respectively (Chen et al. 2022a, b, c; Zhang et al. 2021a, b). Finally, the grid cover area is set within the range of 25.83–43.13°N and 75.40–111.59°E, and grid cells of 1° × 1° were contained in the study. PSCF model divides the research area into i × j grids, and n<sub>ij</sub> is mean the number of all trajectories passing through the grid (i, j), m<sub>ij</sub> is the number of pollution trajectories, PSCF<sub>ij</sub> (the occurrence probability of pollution track in grid (i, j)) is expressed an Eq 0.7 (Bai et al. 2021a, b; Berriban et al. 2022).

$$PSCF_{ij} = \frac{m_{ij}}{n_{ij}} \tag{7}$$

Besides, W<sub>ij</sub> (weight factor) is used to calculate PSCF to reduce uncertainty (Zhang et al. 2022a, b, c; Zhou et al. 2023). By counting the number of all trajectory nodes and the total number of grids, the average number of nodes per grid is obtained, which is defined as n<sub>ave</sub>, then the calculation formula of:

$$W_{ij} = \begin{cases} 1.00, (n_{ij} > 3n_{ave}) \\ 0.70, (1.5n_{ave} < n_{ij} \leq 3n_{ave}) \\ 0.42, (n_{ave} < n_{ij} \leq 1.5n_{ave}) \\ 0.2, (n_{ij} \leq n_{ave}) \end{cases} \tag{8}$$

The PSCF value after adding the weight can be expressed as Eq 0.9:

$$WPSCF_{ij} = W_{ij} \times PSCF_{ij} = W_{ij} \times \frac{m_{ij}}{n_{ij}} \quad (9)$$

**CWT model** The study area set in the CWT model calculation almost covers the entire airflow transport path, with a resolution of  $1.0^\circ \times 1.0^\circ$ . In addition, the threshold settings for  $PM_{2.5}$  and  $O_3$  in the CWT model are consistent with those in PSCF. The weighted concentration of each grid cell is  $C_{ij}$  (Eq 0.10) (Bai et al. 2021a, b; Cao et al. 2023):

$$C_{ij} = \frac{\sum_{l=1}^m C_l \tau_{ijl}}{\sum_{l=1}^m \tau_{ijl}} \quad (10)$$

In the formula,  $i$  and  $m$  represent the trajectory index and the total number of trajectories, respectively.  $C_l$  is the corresponding pollutant concentration when the trajectory  $l$  passes through the grid unit  $(i, j)$ , and  $\tau_{ijl}$  is the trajectory in the grid unit  $(i, j)$  Duration of stay. The same weight factor  $W_{ij}$  as PSCF were used in the study to reduce the uncertainty of CWT. A cell with a higher Weighted Concentration Weighted Trajectory (WCWT) value indicates a greater contribution to the pollutant concentration (Cao et al. 2023; Tian et al. 2022) (Eq 0.11).

$$C_{ij} = \frac{W_{ij}}{\sum_{l=1}^m \tau_{ijl}} \sum_{l=1}^m C_l \tau_{ijl} \quad (11)$$

## Results and discussion

### Spatial and temporal heterogeneity of pollutants

#### Spatial heterogeneity of pollutants

Concentrations of air pollutants are not always at a steady level, but is characterized by multiple temporal and spatial scales. In 2014, the areas with high average concentration of  $PM_{2.5}$  were mainly concentrated in the central urban area, while the low-value region were distributed in Dujiangyan (Fig. S3). In addition, the central region (Wuhouqu, Jinjiang and Shuangliu etc.) is a high CO value area. This finding is similar to those of Kuang et al., (2018), they pointed out that lots of automobiles and industrial enterprises in the central area of Chengdu are the reasons for the higher average CO concentration. On the contrary, the high-value areas of  $O_3$  are mainly concentrated in Dujiangyan and Pengzhou, while the central urban areas are relatively low. In 2015, the pollutants  $PM_{2.5}$ ,  $PM_{10}$ ,  $NO_2$  and CO all gradually decreased from the central urban area to the east and west, and the low-value areas all appeared in Dujiangyan (Fig. S4). While, the distribution characteristics of  $SO_2$  and  $O_3$  concentration values

are characterized by lower values in the central urban area and higher values in the northwest direction. In addition, the  $SO_2$  concentration is higher in the northwest, mainly because there are a large number of industries and power plants in these areas (Kuang et al., 2018). The high-concentration area of  $O_3$  presents a zonal distribution in the northwest direction and is mainly caused by motor vehicle emissions in the central urban region, and in the northern region the impact of industry on  $O_3$  is more important.

Compared with 2014, the  $PM_{2.5}$  concentration in 2016 has improved to a certain extent, and the value in most areas is higher than  $53.6 \mu\text{g}/\text{m}^3$  (Fig. S5). In addition, compared with 2015, the area with high  $NO_2$  and  $O_3$  concentration showed an expanding trend. It may be due to the substantial increase in VOCs emissions in industrialized areas, which facilitated the reaction with  $NO_x$  (Kuang et al., 2018). Zhou et al., (2021) identified that OVOCs emitted from wood-based panels, furniture manufacturing, pharmaceutical industries and automobile manufacturing accounted for more than 50% of Chengdu. Therefore, controlling the emission of VOC in the manufacturing industry is the key to improving the  $O_3$  concentration. In 2017, the high-value areas of  $PM_{2.5}$  and  $PM_{10}$  has shown a trend of shrinking compared with 2014–2016 (Fig. S6). However, the overall pollution is still relatively serious, and the central urban area is still a key area for emission reduction. Air pollutants have serious impacts on human health, and the lethal effects are mainly manifested in total mortality, respiratory diseases, cardiovascular diseases and lung cancer (Alexeeff et al. 2022; Dimitriou et al. 2022). Therefore, it is particularly necessary to reduce pollutant emissions.

Except for  $O_3$ , the concentration values of other pollutants show a decreasing trend in 2018 (Fig. S7). In total, about 98.0% of the region's  $PM_{2.5}$  concentration values failed to reach the limit of CAAQS Grade II. The areas with the highest concentration are Wuhou, Jinjiang, Shuangliu and Qingyang, which is 10 times higher than the WHO, 2021AQGs standard. Xu et al. (2024) pointed out that  $PM_{2.5}$  pollution is a major environmental risk factor that can bring about huge disease burden and economic losses (Xu et al. 2024). Song et al., (2022a, b) emphasized that the formation of secondary aerosols (43.4%) in the winter of 2018 was the main cause of the high concentration of  $PM_{2.5}$ . The central urban area is also a heavily polluted area of  $PM_{10}$ , which is consistent with the observations of Qi et al., (2022) and Luo et al., (2020). Numerous studies have shown that air particulate matter is one of the main causes of mortality, lung and cardiovascular complications, and its long-term effects on the human body are more serious than short-term effects (Alexeeff et al. 2022; Liu et al. 2020a, b; Xu et al. 2024). Therefore, controlling particulate matter has great health benefits. Overall, in 2019 each pollutant showed a certain downward trend compared with 2018, but the distribution characteristics were basically the same (Fig. S8).  $NO_2$  is still the key object of pollutant emission reduction. The research of Qi et al., (2022) also emphasized that the rapid development of urbanization in Chengdu-Chongqing region led to the gradual increase of motor vehicles, which is

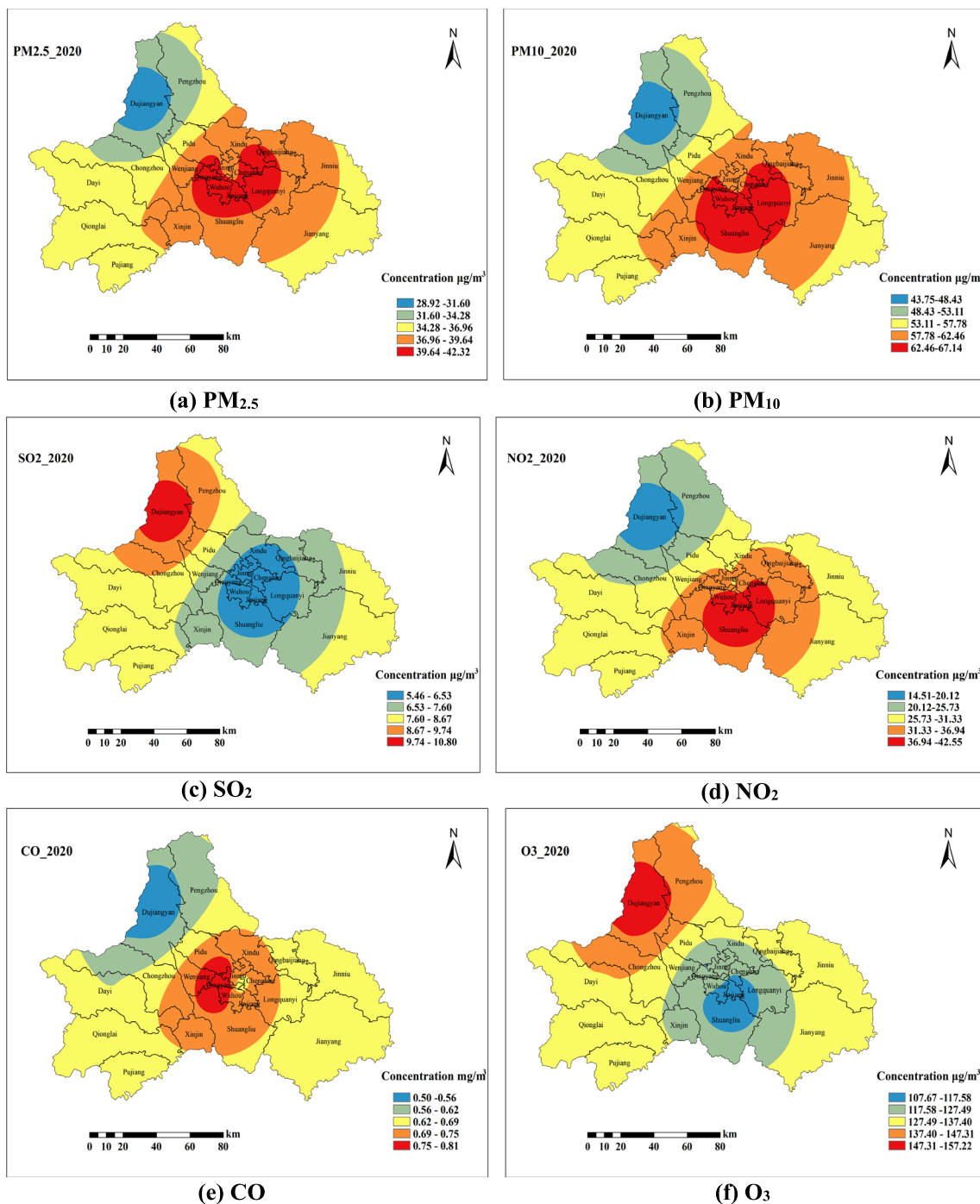


Fig. 5 Spatial variations of six pollutants in 2020

one of the main contributors of NO<sub>2</sub>. About 98.0% of the regions have O<sub>3</sub> concentrations exceeding the limit of WHO, 2021AQGs standards. This result was similar to the findings of Chen et al., (2022a, b, c), Which also underscore that vehicle exhaust and solvent utilization contributed more to O<sub>3</sub> production. O<sub>3</sub> is produced by photochemical reactions of precursors such as NOx and VOCs, so the O<sub>3</sub> concentration depends largely on the VOC/NOx value.

In 2020, except for SO<sub>2</sub> and O<sub>3</sub>, the distribution characteristics of other pollutants are generally larger in the central urban area (Fig. 5). The areas with high PM<sub>2.5</sub> values are distributed in the northwest of the central urban region, and gradually decrease eastward and westward. The concentration of NO<sub>2</sub> is higher in the south of the central urban area, and gradually decreases eastward and westward from this center. This may be due to the high urbanization and high motor vehicle emissions in the central

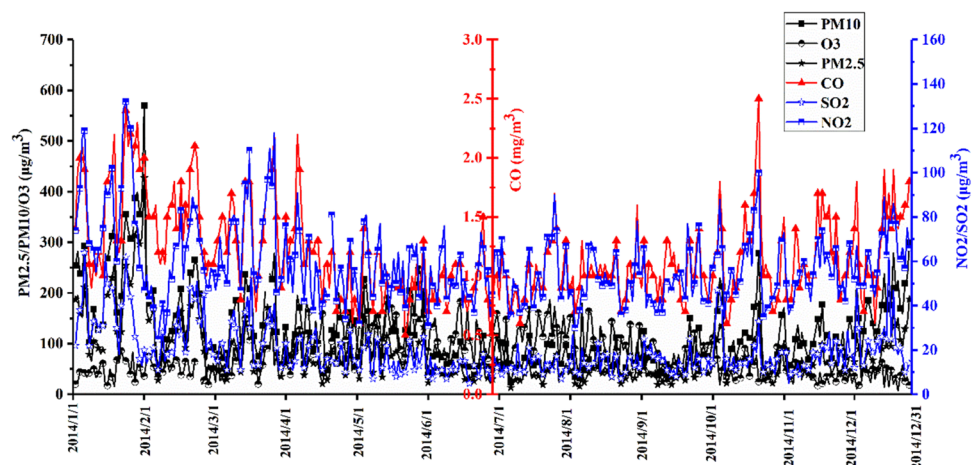
region. The average value of  $O_3$  has increased slightly, and the average value in 2020 is  $169 \mu\text{g}/\text{m}^3$ , which is lower in the central region and relatively higher in the new cities in the eastern and western suburbs. It is intriguing that, compared with 2019, during the lockdown of COVID-19 in 2020, except for  $O_3$  showing a slight increase trend, the concentration values of other pollutants decreased significantly, which may be due to the reduction in emissions, rather than due to the meteorological conditions with a large range (Gao et al. 2023; Konstantinou et al. 2021; Xia et al. 2022). Overall, all pollutants in each region showed a decrease trend from 2014 to 2020, except for the  $O_3$  concentration which showed a certain fluctuation and growth. The spatial patterns of pollutants ( $PM_{2.5}$ ,  $PM_{10}$ , CO,  $NO_2$ ) all show higher concentrations in the central region. This may be due to frequent human activities and high emissions from industrial and vehicles in the central urban area (Tan et al. 2023; Zhu et al. 2019). While,  $O_3$  and  $SO_2$  showed a relatively low distribution pattern in the central urban area. Overall, the air pollution in Chengdu from 2014 to 2020 showed the characteristics of both high  $PM_{2.5}$  and  $O_3$  concentrations. This is generally similar to the findings of the Qi et al., (2022) and Tan et al., (2023), which emphasized that

high concentrations of PM and  $O_3$  are closely related to dense traffic flow and basin topography. In addition, existing studies have shown that  $PM_{2.5}$  and  $O_3$  are the main pollutants in most cities. High concentrations of  $PM_{2.5}$  and  $O_3$  may pose a huge threat to public health and are closely related to premature death (Gómez González et al. 2023; Liu et al. 2022). Some studies have also shown that strategies to reduce  $PM_{2.5}$  concentrations may change the  $NO_x$ -VOC ratio, thereby, adversely affecting the control of  $O_3$  (Liang et al. 2021; Xu et al. 2023). Therefore, it is particularly important to further explore the complex relationship, sources and health effects of  $PM_{2.5}$  and  $O_3$ .

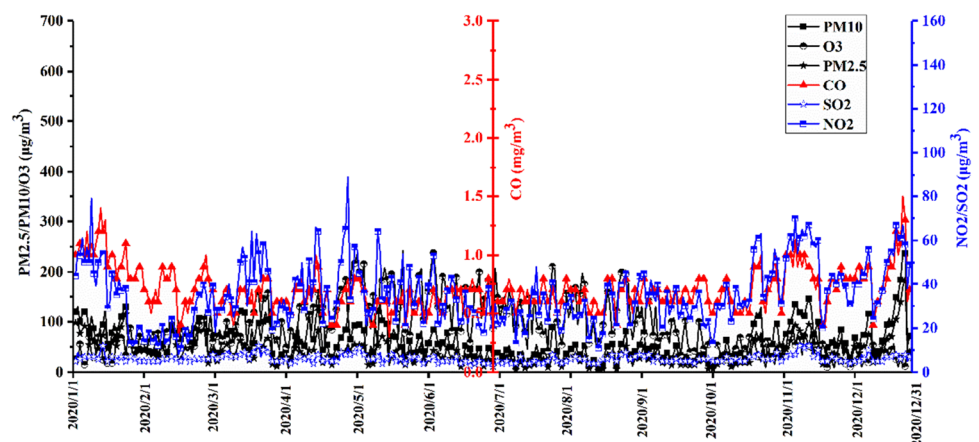
### Temporal variation characteristics of pollutants

Based on the spatial distribution characteristics, it can be concluded that the pollutant concentration in Chengdu showed a downward trend from 2014 to 2020, and the air quality has been significantly improved. The daily concentration variation characteristics of six pollutants in 2014 and 2020 are shown in Fig. 6 and Fig. 7. It can be seen that the pollutant concentration values in 2014 were

**Fig. 6** Temporal variations of six pollutants in 2014



**Fig. 7** Temporal variations of six pollutants in 2020





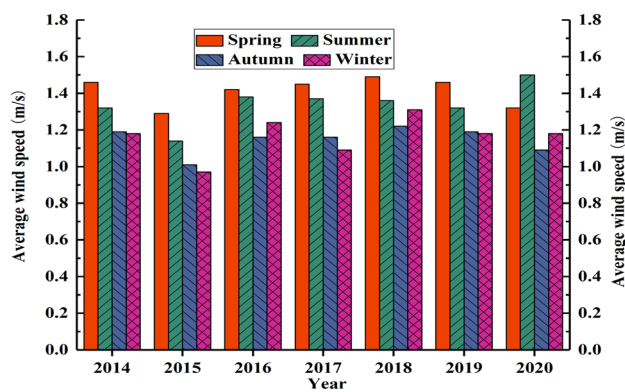


**Fig. 8** Seasonal Wind speed

significantly higher than those in 2020, which is obviously related to the epidemic control measures in 2020 (Bashir et al. 2020; Qi et al. 2022). Among them,  $\text{SO}_2$ , CO,  $\text{NO}_2$  and  $\text{PM}_{2.5}$  decreased more significantly, but the concentrations of  $\text{O}_3$  and  $\text{PM}_{2.5}$  were still high. It can be seen from the figure that the particle concentration values are higher in autumn and winter, while the  $\text{O}_3$  concentration values are higher in summer. This is consistent with the research results of Lu et al., (2022a, b), that is,  $\text{PM}_{2.5}$  shows a "U"-shaped change trend, while  $\text{O}_3$  shows an inverted "U"-shaped variation characteristic. High concentrations of  $\text{O}_3$  can lead to the formation of photochemical smog pollution, and long-term exposure to high concentrations of  $\text{O}_3$  will not only harm human health, but also have an adverse effect on plant growth and crop yields (Chen et al. 2022a, b, c; Wang et al. 2022a, b). Therefore, in winter, the control of precursors such as  $\text{SO}_2$ ,  $\text{NH}_3$  and primary  $\text{PM}_{2.5}$  should be strengthened in a coordinated manner to achieve coordinated prevention and control of  $\text{PM}_{2.5}$  and  $\text{O}_3$ . In addition, the atmospheric environment is already in the transition stage from primary pollution to secondary pollution. While controlling primary pollution, it is necessary to prevent the occurrence of secondary pollution (Liang et al. 2023a, b; Mostafa et al. 2021; Zhang et al. 2023).

## Influence of meteorological parameters on the air pollutants

### Variation characteristics of meteorological factors

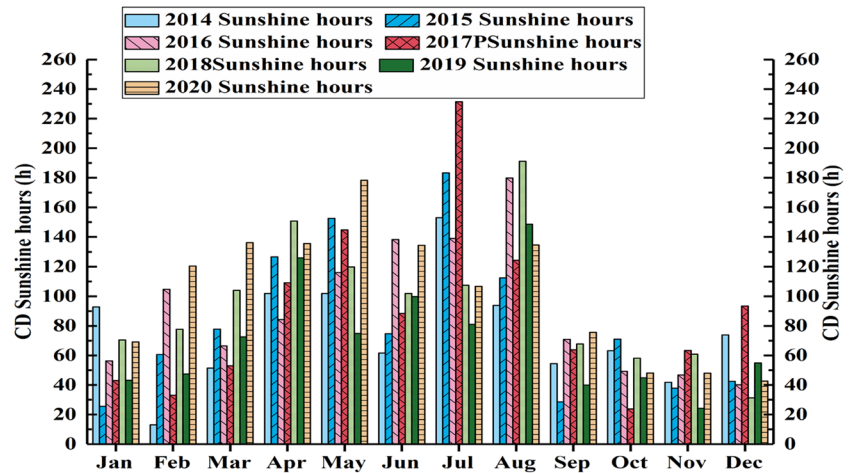
**Wind speed and sunshine duration** Wind affects the diffusion and transportation of air pollutants, and plays a prominent role in the spatial distribution of air pollution. Chengdu is located in the SCB, with low wind speed all year round. The annual average wind speed between 2014

and 2020 is 1.0 m/s, 1.1 m/s, 1.3 m/s, 1.27 m/s, 1.35 m/s, 1.29 m/s, 1.27 m/s, respectively, all lower than 1.4 m/s. Overall, there are seasonal differences in wind speed during the study period, with larger values appearing in spring and summer (Fig. 8), and the highest values appearing in April–August (Fig. S9). Besides, a notable characteristic of the climate in Chengdu is cloudy with short sunshine hours. During the study period, the average annual sunshine duration was 1,038 h, and the average annual sunshine duration in 2019 was the lowest (857 h). Obvious seasonal differences can be found in the sunshine hours, with the largest values in spring and summer every year. The longest sunshine time in each year is mainly concentrated in April–August (Fig. 9).

**Relative humidity and precipitation** Fluctuations in relative humidity can affect atmospheric stability and lead to changes in pollutant concentrations. There are some differences in the average relative humidity and minimum relative humidity of various meteorological stations in Chengdu. The average relative humidity is between 68% and 88.6%, and most sites are higher than 70% (Fig. 10). The annual average relative humidity is 79.6%, and the minimum value is about 54.4%. The relative humidity shows seasonal variations, which are relatively high in autumn and winter and generally low in spring (Fig. S10). The seasonal heterogeneity of relative humidity is also one of the main bases for explaining the seasonal variation of pollutants. In addition, the maximum relative humidity is concentrated in September to December, all higher than 80%, and the minimum value occurs in February to April in most years. Precipitation is also one of the main parameters affecting the concentration of atmospheric pollutants, and wet deposition can clean the atmospheric pollutants (Jia et al. 2019; Wang et al. 2016). During 2014–2020, the precipitation at each station was inconsistent, and the precipitation was relatively high at Dujiangyan station and Pujiang station (Fig. 11). There are obvious differences in precipitation in different seasons, and the overall trend is "inverted U shape" (Fig. S11). Summer precipitation is obviously higher than other seasons, and winter is the lowest. The precipitation is mainly concentrated in July and August, and the precipitation in November, December, January and February is relatively small (Fig. S12).

**Temperature, ground surface temperature and pressure** The transport and distribution of regional air pollutants are obviously affected by temperature. Higher temperature can enhance the thermodynamic conditions of the atmosphere, intensify the turbulent exchange of the atmosphere, and promote the vertical diffusion and horizontal transport of the atmosphere (Li et al. 2021; Zhan et al. 2019). From 2014 to 2020, the average temperature of each station is basically the same, about 17 °C (Fig. S13).

Fig. 9 Monthly SSD



The daily maximum temperature values at each site were lower than 25 °C, and the minimum temperature fluctuated between 12.5 °C and 15 °C. The annual average temperature is around 16.4 °C to 17.6 °C, with the highest value in summer and the lowest in winter (Fig. 12). The average monthly temperature in each year presents an inverted “U-shaped” change pattern. The highest average temperature appears in July and August, and the extreme minimum temperature appears in January, which is -6.7 °C.

From 2014 to 2020, the annual changes of GST are relatively stable, and the annual average is about 17 °C. In addition, GST showed an inverted “U-shaped” seasonal variation in each year (Fig. S14). The monthly variation trend of GST in each year is similar, showing an inverted “U shape”. The average maximum GST occurs in July and August and the maximum GST occurs in May–August (Fig. 13). In general, the PRS annual value fluctuation of range is 946 hPa–956 hPa. High atmospheric pressure values are mainly concentrated in winter and lowest in summer. The monthly trends of each year from 2014 to 2020 are consistent, showing a “U-shaped” trend, with the maximum values concentrated in January, February and December, and the minimum values appearing in June and July (Fig. S15).

### Relationship between PM pollutants and meteorological factors

The relationship between meteorological factors and PM concentration is not a simple linear relationship, and each meteorological factor has different correlations with air quality conditions. It can be seen from Table 3 that among the meteorological parameters, only PRS is positively correlated with the concentrations of PM<sub>2.5</sub> and PM<sub>10</sub>. Wind is a meteorological parameter closely related to the level of air pollution, and it plays a positive role in the dilution and transport

of air pollutants (Flores et al. 2020; Peng et al. 2022; Zhan et al. 2019). It is clear that that wind is negatively correlated with PM<sub>2.5</sub> and PM<sub>10</sub>, and the correlation coefficients are -0.445 and -0.427, respectively (Table 3). Furthermore, a significant negative correlation between wind speed and PM was also observed in summer, indicating that higher wind speed can accelerate the dilution of PM, thereby reducing PM concentration (Fig. 14). On the contrary, the static and steady wind will increase the mass concentration of PM. Besides, PM<sub>2.5</sub> and PM<sub>10</sub> had a significant negative correlation with air temperature, with correlation coefficients of -0.730 and -0.697, respectively, indicating that high temperature is also conducive to reducing PM concentration. Relevant studies have shown that one of the main reasons for the serious air pollution in the Chengdu Plain in winter is the high frequency of temperature inversions in winter and the weak intensity of cold air, which makes it difficult for pollutants to diffuse in the basin (Kong et al. 2020). High relative humidity is conducive to the secondary transformation of precursors and the retention of atmospheric particulate matter in the air, thereby promoting the chemical transformation and hygroscopic growth of aerosols (Kong et al. 2020). The findings of Fan et al. (2021) also found that the ratio of PM<sub>2.5</sub>/PM<sub>10</sub> tends to be higher in southern Chinese cities due to higher relative humidity in winter. Kong et al. (2020) found that secondary aerosol is an important source of PM<sub>2.5</sub> in Chengdu, which is sensitive to meteorological factors.

In the absence of precipitation, relative humidity is generally positively correlated with PM<sub>2.5</sub> concentrations (Fan et al. 2021; Li et al. 2019a, b). There was a negative correlation between PM and RHU (PM<sub>2.5</sub>:R = -0.257, PM<sub>10</sub>:R = -0.334). The correlation is extremely strong in summer, indicating that relative humidity has the most significant effect on PM in summer. Between 2014 and 2020, PM<sub>2.5</sub> and PM<sub>10</sub> showed a negative correlation with PRE (PM<sub>2.5</sub>:R = -0.505, PM<sub>10</sub>:R = -0.521), indicating that rainfall

Fig. 10 RHU in the station

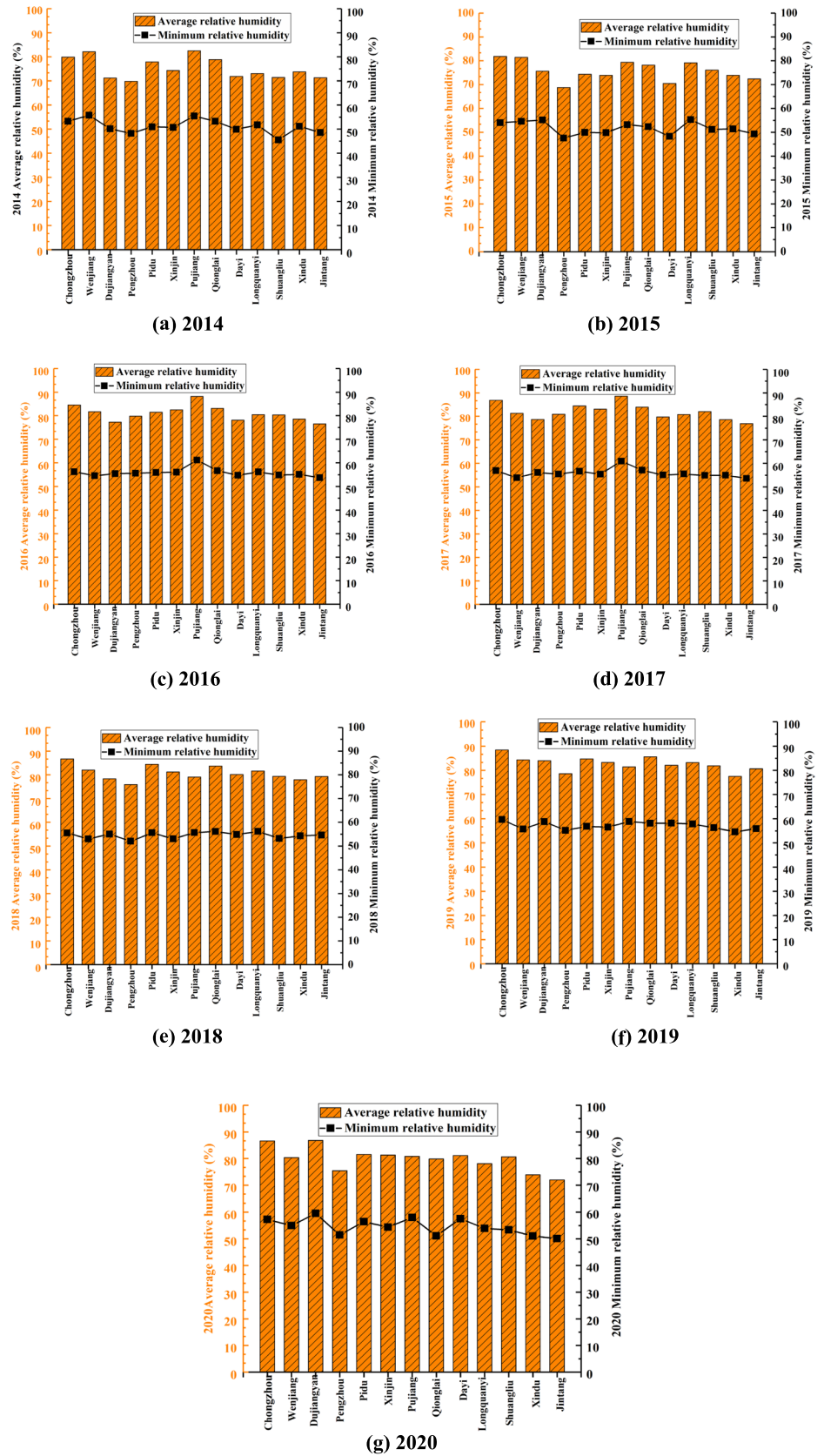


Fig. 11 Annual PRE

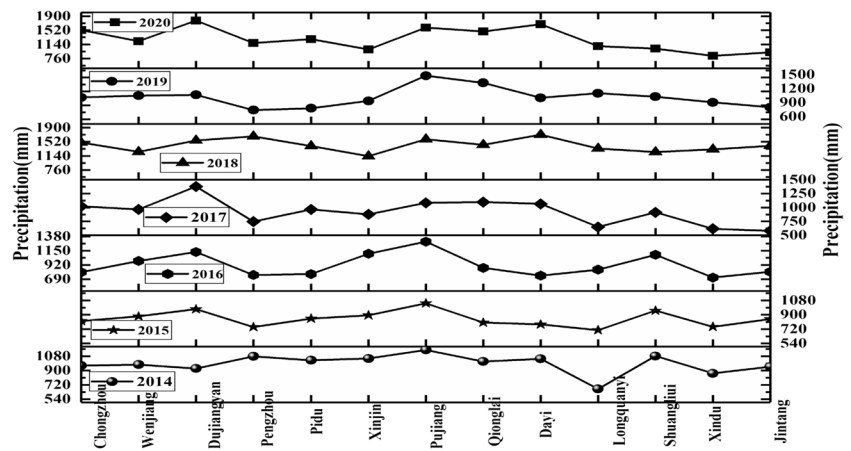
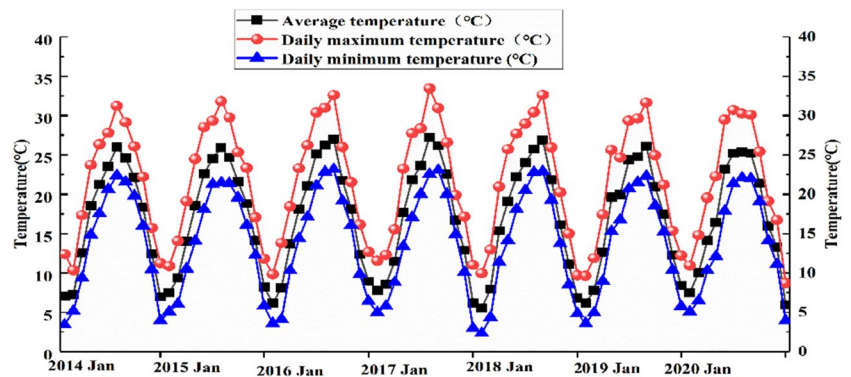


Fig. 12 Monthly TEM



can reduce the concentration of PM. The increase in precipitation accelerates the wet removal of pollutants, which in turn reduces the concentration of pollutants (Yang et al. 2019a, b). Most of the rainfall in Chengde is concentrated in summer, when the concentration of PM is the lowest (Huang et al. 2015; Liu et al. 2018). The correlation coefficients between PRE and  $PM_{2.5}$  and  $PM_{10}$  in summer reached -0.598 and -0.669, respectively. Furthermore, PM concentration was also affected by SSD, showing a negative correlation between them ( $PM_{2.5}:R=-0.375$ ,  $PM_{10}:R=-0.332$ ). The higher the SSD, the higher the temperature will be, which is more conducive to the secondary conversion of PM. The fluctuation of PM concentration is opposite to that of GST (Fig. 14), and there is a significant negative correlation between them ( $PM_{2.5}:R=-0.724$ ,  $PM_{10}:R=-0.668$ ). Overall, particulate matter was only positively correlated with PRS ( $PM_{2.5}:R=0.654$ ,  $PM_{10}:R=0.638$ ), indicating that an increase in air pressure would promote an increase in PM concentration. The downward airflow generated by high pressure can inhibit the upward movement of PM, leading to particle accumulation, which is more obvious in winter. In general, weather conditions such as strong wind, high temperature, and low humidity can promote the dilution and diffusion of particulate matter, which is promote the reduction of particulate matter concentration.

### Relationship between gaseous pollutants and meteorological factors

Wind facilitates the dispersion and transport of pollutants. It can be observed that  $SO_2$ ,  $NO_2$ , and CO all illustrated negative correlations with wind speed, and the correlation coefficients are -0.412, -0.401 and -0.475, respectively (Table 4). However, there was a significant positive correlation between  $O_3$  and wind speed ( $R=0.624$ ). The possible reason is that higher wind speed can dilute PM and enhance solar radiation, thus accelerating the formation of  $O_3$  (Romshoo et al. 2021; Yang et al. 2020; Zhang et al. 2015).  $SO_2$ , CO and  $NO_2$  were only positively correlated with PRS, and showed different negative correlations with other meteorological factors (Table 4). Furthermore, it can be observed that  $O_3$  is only negatively correlated with RHU and PRS. In addition, the concentration of  $SO_2$ ,  $NO_2$  and CO is relatively low when the TEM is high, while the fluctuation of  $O_3$  is basically consistent with the TEM and presents an “inverted U-shape” (Fig. 15). This is consistent with the correlation shown in Table 4,  $SO_2$ ,  $NO_2$  and CO have different negative correlations with TEM, and the correlation is:  $CO > NO_2 > SO_2$ . However, a strong positive correlation was observed between  $O_3$  and TEM ( $R=0.827$ ), studies also shown that high temperatures are one of the factors leading to severe ozone

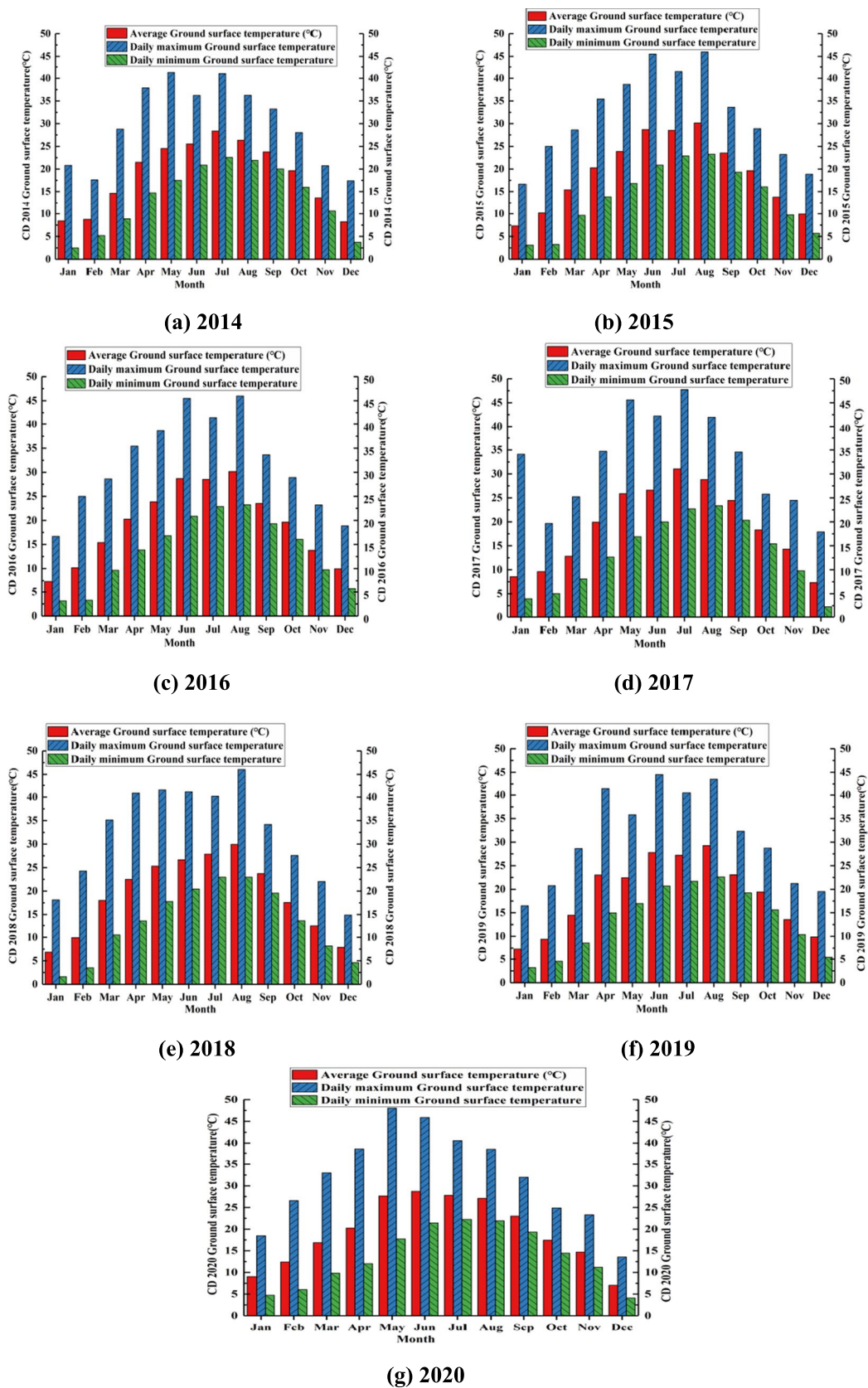


Fig. 13 Monthly GST between 2014 and 2020

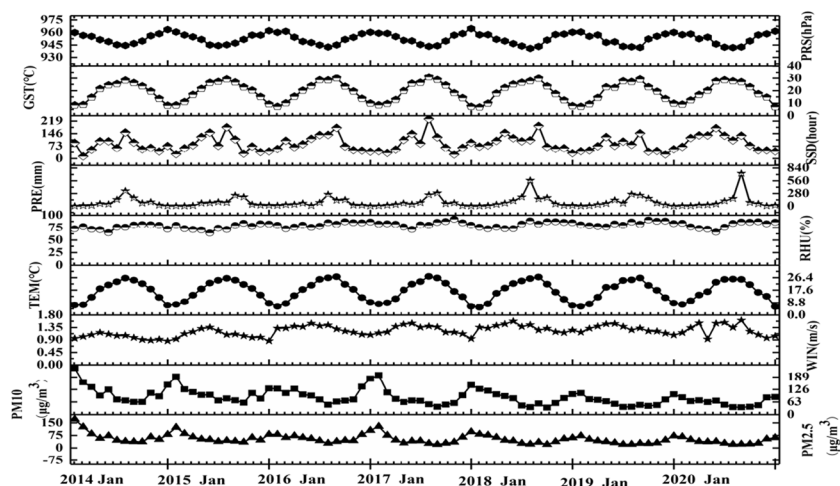
**Table 3** Correlation between PM and meteorological factors in Chengdu

Pollutants	WIN	TEM	RHU	PRE	SSD	GST	PRS
Yearly							
PM <sub>2.5</sub>	-0.445	-0.730	-0.257	-0.505	-0.375	-0.724	0.654
PM <sub>10</sub>	-0.427	-0.697	-0.334	-0.521	-0.332	-0.688	0.638
WIN		0.370	-0.117	0.322	0.496	0.405	-0.538
TEM			0.017	0.638	0.619	0.996	-0.930
RHU				0.282	-0.439	-0.048	0.091
PRE					0.379	0.610	-0.661
SSD						0.665	-0.668
GST							-0.938
Spring							
PM <sub>2.5</sub>	0.075	0.142	-0.413	-0.040	-0.461	-0.039	0.146
PM <sub>10</sub>	-0.011	0.239	-0.4600	-0.030	-0.394	0.055	0.086
WIN		-0.226	0.593	0.492	-0.560	-0.477	-0.076
TEM			-0.394	0.217	0.569	0.909	-0.727
RHU				0.731	-0.423	-0.610	-0.273
PRE					-0.363	-0.143	-0.765
SSD						0.807	-0.238
GST							-0.507
Summer							
PM <sub>2.5</sub>	-0.622	0.024	-0.810	-0.598	-0.042	-0.267	0.268
PM <sub>10</sub>	-0.691	-0.035	-0.859	-0.669	-0.044	-0.240	0.278
WIN		0.094	0.716	0.710	0.244	0.208	0.160
TEM			0.169	0.050	0.117	0.168	-0.128
RHU				0.551	0.373	0.499	-0.528
PRE					-0.100	-0.234	0.178
SSD						0.899	-0.142
GST							-0.373
Autumn							
PM <sub>2.5</sub>	-0.131	0.694	-0.588	-0.106	0.492	0.647	-0.729
PM <sub>10</sub>	-0.179	0.736	-0.633	-0.099	0.505	0.685	-0.764
WIN		-0.638	0.451	0.011	-0.284	-0.567	0.294
TEM			-0.678	-0.009	0.331	0.969	-0.717
RHU				-0.031	-0.391	-0.486	0.509
PRE					-0.827	-0.005	0.534
SSD						0.256	-0.788
GST							-0.711
Winter							
PM <sub>2.5</sub>	-0.317	-0.055	-0.718	-0.130	-0.305	-0.246	0.653
PM <sub>10</sub>	-0.258	-0.032	-0.680	0.028	-0.322	-0.241	0.711
WIN		-0.762	-0.113	0.199	0.576	-0.555	-0.405
TEM			0.383	0.298	-0.155	0.932	0.514
RHU				0.273	0.149	0.352	-0.172
PRE					0.589	0.342	0.428
SSD						0.097	-0.022
GST							0.352

pollution (Qiao et al. 2021; Yang et al. 2020). The photochemical reaction rate in the troposphere is significantly accelerated by high temperature, which promotes the conversion rate between O<sub>3</sub> and precursors, thereby generating abundant O<sub>3</sub> (Kong et al. 2020; Kuang et al., 2018).

Existing research has emphasized that pollutants tend to accumulate under conditions of high relative humidity and promote various secondary processes, further exacerbating regional air pollution (Li et al. 2022a, b; Ma et al. 2022). The gaseous pollutants showed different

**Fig. 14** The relationship between PM ( $PM_{10}$ ,  $PM_{2.5}$ ) and meteorological factors



negative correlations with RHU. Besides,  $SO_2$ ,  $NO_2$  and CO displayed different negative correlations with PRE, and the correlation was  $NO_2 > CO > SO_2$ . However, a positive correlation can be observed between  $O_3$  and PRE ( $R = 0.457$ ), indicating that precipitation was beneficial to the accumulation of  $O_3$ .  $O_3$  is also greatly affected by SSD and shows a strong positive correlation ( $R = 0.819$ ). Because the sun's ultraviolet radiation is strong when there is sufficient sunshine, it is very conducive to the photochemical reaction to generate  $O_3$ . In winter, solar radiation is significantly weakened, and the scattering and absorption of high-concentration particulate matter slows down the production of  $O_3$  (Kuang et al., 2018; Lu et al. 2022a, b). In addition, the significant negative correlations can be found between sunshine duration and pollutants  $SO_2$ ,  $NO_2$ , and CO. In winter, except for  $O_3$ , other pollutants' concentration in this region is relatively high.  $SO_2$ ,  $NO_2$  and CO all expressed a significant negative correlation with GST, and there were seasonal differences in the correlation. On the contrary, it can be found that  $O_3$  has a strong positive correlation with GST ( $R = 0.863$ ), which is consistent with the change trend shown in Fig. 15. This indicates that the increase in temperature is beneficial to the formation of  $O_3$ . It can be observed that the concentrations of  $SO_2$ ,  $NO_2$  and CO are only positively correlated with PRS (Table 4). While,  $O_3$  showed a strong negative correlation with PRS ( $R = -0.894$ ). Under low pressure conditions, it is easy to form a static and stable weather pattern, which in turn leads to a surge in regional  $O_3$  pollutants (Yang et al. 2020). Overall,  $O_3$  concentrations were only significantly negatively correlated with RHU and PRS. In addition, the reduction rate of VOC and  $NO_x$  was proved to be the main way to reduce  $O_3$  and  $PM_{2.5}$  emissions in Chengdu (Kuang et al., 2018).

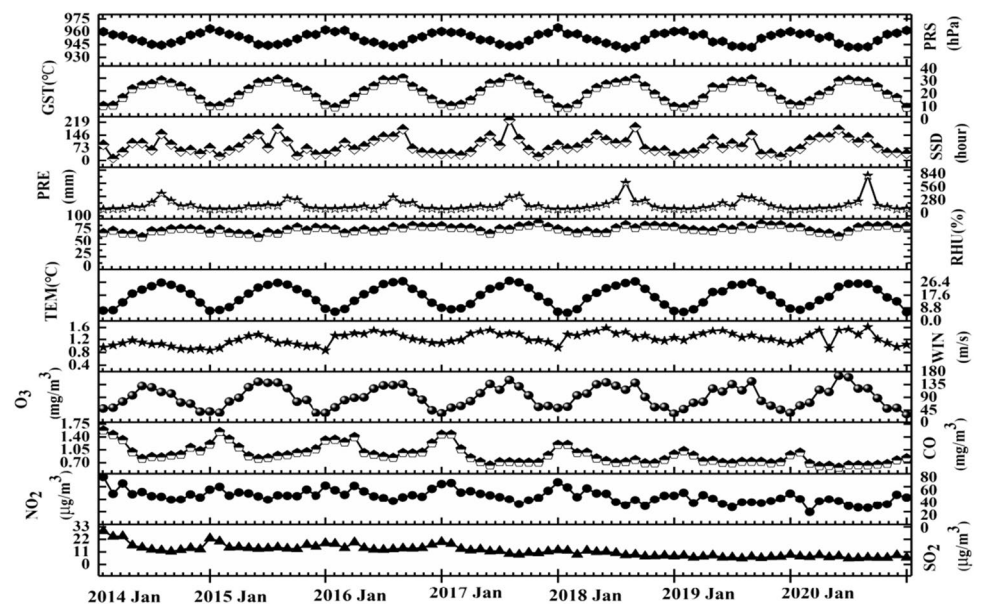
## Pollution trajectory and potential source analysis

### Back trajectory cluster analysis

Cluster analysis can not be done by only derive different classes of trajectories, but also provide valuable information for identifying the history of air masses and air pollution in specific regions (Berriban et al. 2022; Yu et al. 2019). According to the track direction and transport area distribution, the trajectories of air masses in 2020 were divided into different clusters in the four seasons (Fig. 16). In spring, air mass trajectories are clustered into seven categories, among which cluster C2 has the longest trajectory, accounting for 9.22%. Clusters C1, C5, and C6 are all from the northeast of Chengdu, accounting for 14.85%, 13.67% and 10.45%, respectively. Cluster C3 has a shorter track length but the largest proportion (30.61%). In summer, the trajectories are clustered into four categories, among which cluster C2 has the fastest transport speed, accounting for 18.98%, mainly from the northeast direction of the acceptor point. The one with the shortest track length is cluster C3, accounting for the largest proportion (33.06%). Cluster C1 is mainly transported in Chongqing and Guiyang, accounting for 26.20%. In addition, shorter air masses indicate that the air mass moves slowly and is prone to accumulation of pollutants (Berriban et al. 2022; Zhan et al. 2019). Cluster C2 is the largest among the six types of trajectories in autumn, accounting for 25.57%. The longest trajectory is cluster C6, which mainly comes from the southwest direction of Xi'an. Cluster C3 has the shortest trajectory length, indicating that the air mass moves slowly and the pollutants are mainly emitted locally. Most of the trajectories in autumn originated from the north and northeast (Xi'an, Lanzhou, Chongqing). In winter, the trajectory cluster C2 accounted for 28.05%, with the longest trajectory length. It shows that

**Table 4** Correlation between gaseous pollutants and meteorological factors in Chengdu

Pollutants	WIN	TEM	RHU	PRE	SSD	GST	PRS
Yearly							
SO <sub>2</sub>	-0.412	-0.299	-0.354	-0.286	-0.182	-0.303	0.309
NO <sub>2</sub>	-0.401	-0.548	-0.276	-0.478	-0.276	-0.546	0.559
CO	-0.475	-0.614	-0.153	-0.381	-0.408	-0.625	0.568
O <sub>3</sub>	0.624	0.827	-0.389	0.457	0.819	0.863	-0.894
Spring							
SO <sub>2</sub>	0.107	-0.056	-0.372	-0.165	-0.529	-0.210	0.393
NO <sub>2</sub>	0.415	0.088	-0.121	0.126	-0.522	-0.182	0.150
CO	0.154	0.087	-0.130	0.247	-0.617	-0.192	-0.001
O <sub>3</sub>	-0.455	0.746	-0.460	-0.245	0.964	0.914	-0.382
Summer							
SO <sub>2</sub>	-0.648	0.094	-0.682	-0.684	0.224	0.024	0.100
NO <sub>2</sub>	-0.722	-0.122	-0.690	-0.742	0.062	-0.090	-0.031
CO	-0.627	0.259	0.262	-0.108	0.576	0.736	-0.072
O <sub>3</sub>	0.028	0.224	0.262	-0.108	0.576	0.736	-0.072
Autumn							
SO <sub>2</sub>	-0.384	0.854	-0.667	-0.006	0.407	0.797	-0.685
NO <sub>2</sub>	-0.386	0.809	-0.445	-0.029	0.340	0.804	-0.609
CO	-0.267	0.787	-0.719	0.051	0.409	0.720	-0.712
O <sub>3</sub>	0.128	-0.061	0.350	-0.295	0.312	0.013	-0.150
Winter							
SO <sub>2</sub>	-0.253	0.057	-0.748	0.046	-0.190	-0.077	0.763
NO <sub>2</sub>	-0.232	-0.050	-0.486	0.052	-0.463	-0.326	0.662
CO	-0.399	0.205	0.203	-0.228	0.004	-0.553	-0.405
O <sub>3</sub>	0.323	-0.578	0.203	-0.228	0.004	-0.553	-0.835

**Fig. 15** The relationship between gaseous pollutants and meteorological factors

the long-distance transportation in winter mainly comes from Xi'an, Lanzhou. The track length of Cluster C3 is the shortest, indicating that the air mass transportation speed is the slowest, and it is mainly local emissions.

### Seasonal PSCF analysis of PM<sub>2.5</sub> and O<sub>3</sub>

Areas with higher WPSCF values have a higher probability of passing pollution trajectories, that is, the trajectories



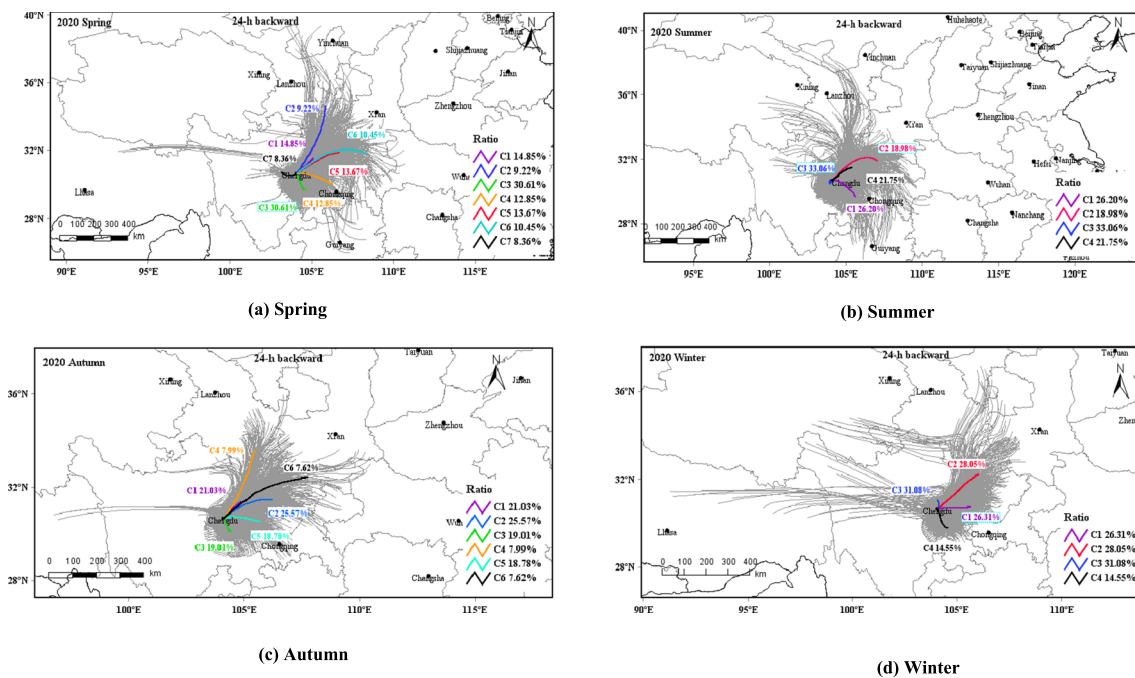


**Fig. 16** Seasonal trajectory cluster in 2020. Note: The gray lines in the figure represent the backward trajectory distribution of external air masses in different seasons

passing through this area are the main transport paths that affect the concentrations of  $\text{PM}_{2.5}$  and  $\text{O}_3$  (Gogikar & Tyagi 2016; Zhou et al. 2023). Through the analysis, it can be observed that the concentration of  $\text{PM}_{2.5}$  in each hour in the summer of 2020 is lower than  $75 \mu\text{g}/\text{m}^3$  and the hourly average concentration of  $\text{O}_3$  in autumn and winter is lower than  $160 \mu\text{g}/\text{m}^3$ . To deeply and quantitatively explore the potential source areas of  $\text{PM}_{2.5}$  and  $\text{O}_3$  in these seasons, the thresholds of  $\text{PM}_{2.5}$  and  $\text{O}_3$  in these seasons were set at  $35 \mu\text{g}/\text{m}^3$  and  $100 \mu\text{g}/\text{m}^3$ , respectively (GB3095-2012). From the PSCF simulation results, it can be observed that the potential source distribution regions of  $\text{PM}_{2.5}$  and  $\text{O}_3$  are different in different seasons. This is mainly due to significant differences in air flow in different seasons. However, the overall distribution of potential source regions is basically consistent with the trajectory transport distribution of air masses.

The potential sources of  $\text{PM}_{2.5}$  in 2020 have obvious seasonal differences, in which the largest WPSCF value appear in winter, and the smallest value occurs in spring and summer (Fig. 17). In spring, the potential sources of  $\text{PM}_{2.5}$  are generally concentrated in the east of Chengdu and the southwest of Xi'an, and the WPSCF values in these areas are all lower than 0.4. The concentration of  $\text{PM}_{2.5}$  in summer is lower than  $75 \mu\text{g}/\text{m}^3$ . Figure 17 (b) shows the potential source areas where  $\text{PM}_{2.5}$  is higher than  $35 \mu\text{g}/\text{m}^3$  but lower than  $75 \mu\text{g}/\text{m}^3$ , and the main contributing

sources are located in the east of Chengdu and the southwest of Chongqing. Local sources dominate in autumn, and the potential source areas of  $\text{PM}_{2.5}$  are mostly concentrated in the east and northeast of Chengdu. In winter,  $\text{PM}_{2.5}$  is affected by regional transport in addition to local contributing sources. The northeastern part of Lanzhou is the main source of contribution, and the WPSCF value is greater than 0.6. In addition, the eastern of Chengdu, the southwestern of Chongqing, and the northern part of Guiyang are the main potential sources of  $\text{O}_3$  in the spring and summer (Fig. S16). The WPSCF value in spring is higher in the southwestern part of Chongqing ( $0.5 < \text{WPSCF} < 0.7$ ), indicating that this area contributes more to  $\text{O}_3$  in spring. The areas with higher WPSCF values in summer are distributed in the northwest of Guiyang, but the overall WPSCF values in summer are lower than 0.4. There is no area with  $\text{O}_3$  concentration higher than  $160 \mu\text{g}/\text{m}^3$  in autumn and winter, but there are some potential source areas higher than  $100 \mu\text{g}/\text{m}^3$  in the central and eastern part of Chengdu ( $\text{WPSCF} < 0.2$ ), indicating that  $\text{O}_3$  concentration is lower in autumn and winter.

### Seasonal CWT analysis of $\text{PM}_{2.5}$ and $\text{O}_3$

CWT model has the advantage of being able to distinguish between regions of high and moderate  $\text{PM}_{2.5}$  and  $\text{O}_3$  concentration. The potential source areas reflected by CWT are more abundant than the PSCF simulation

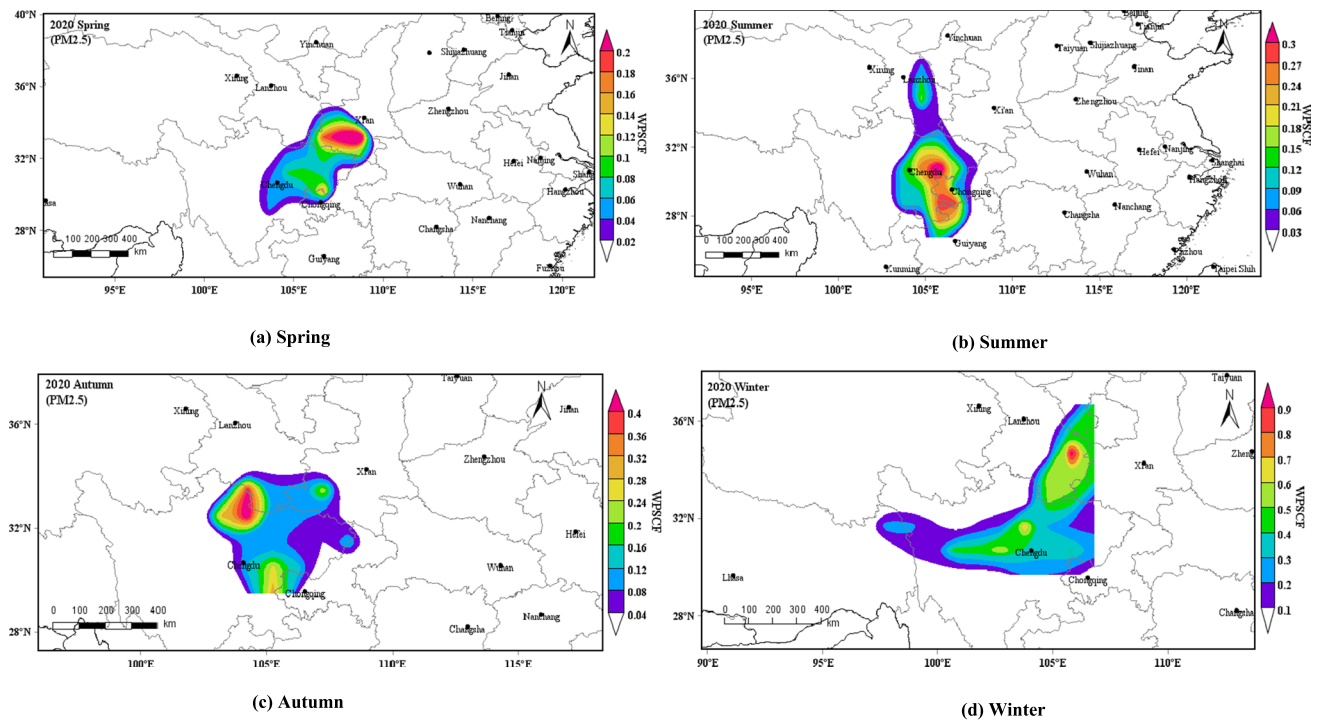


**Fig. 17** Source region of PM<sub>2.5</sub> identified by PSCF in four seasons of 2020

results (Li et al. 2017a, b). Overall, the CWT simulation in 2020 is basically consistent with the PSCF model results, and the potential sources area of PM<sub>2.5</sub> were found in the north of Chengdu and southwest of Chongqing (Fig. 18). However, the potential influence area of the CWT model is larger than that of the WPSCF distribution. The WCWT value was the largest in winter, and the values in all regions were lower in spring and summer. In autumn, the eastern part of Chengdu is the main potential source area, but the WCWT value of the whole potential source area is between 10  $\mu\text{g}/\text{m}^3$  and 50  $\mu\text{g}/\text{m}^3$ . In winter, the WCWT value is larger (higher than 100  $\mu\text{g}/\text{m}^3$ ) in the southeast of Lanzhou, indicating that regional transport has a significant impact on the distribution of PM<sub>2.5</sub>. For O<sub>3</sub>, there are also seasonal differences in the distribution of CWT simulation results in 2020, with wider distribution areas in spring and summer (Fig. S17). The WCWT value in spring is higher than 100  $\mu\text{g}/\text{m}^3$  in most parts of southern Chongqing, indicating that this region is a source of high concentration of O<sub>3</sub>. In summer, the high O<sub>3</sub> concentration source area appears in the border area between western Chongqing and Chengdu. The distribution area of WCWT in autumn and winter is relatively concentrated. The WCWT values in autumn are mainly distributed in the northeast of Chengdu, southwest of Xi'an, west of Chongqing and southeast of Lanzhou. The distribution area of winter simulation results is also small, mainly in the north of Chengdu and the south

of Lanzhou, and the WCWT value is less than 50  $\mu\text{g}/\text{m}^3$ . High concentrations of O<sub>3</sub> will also accelerate the formation of pollutants such as particulate matter, thereby, increasing the frequency and intensity of severe pollution weather. Therefore, PM<sub>2.5</sub> and O<sub>3</sub> pollution prevention and control measures must be spatially and temporally differentiated.

## Conclusions

Scientific emission reduction in complex terrain areas under the goal of coordinated environmental and climate governance is challenging. In this research, the spatial fluctuation characteristics of the six criteria pollutants were investigated, also the relationship between the air pollutants and meteorological factors are explored in detail. And through the backward trajectory model the transmission paths and contribution of potential sources of PM<sub>2.5</sub> and O<sub>3</sub> in Chengdu in 2020 were analyzed. The conclusions and recommendations are as follows:

- (1) The spatial patterns of pollutants (PM<sub>2.5</sub>, PM<sub>10</sub>, NO<sub>2</sub>, CO) all show higher concentrations in the central region. While, O<sub>3</sub> and SO<sub>2</sub> showed a relatively low spatial pattern in the central urban area. Overall, air pollution in Chengdu (2014–2020) was characterized by both high PM<sub>2.5</sub> and O<sub>3</sub> concentrations.

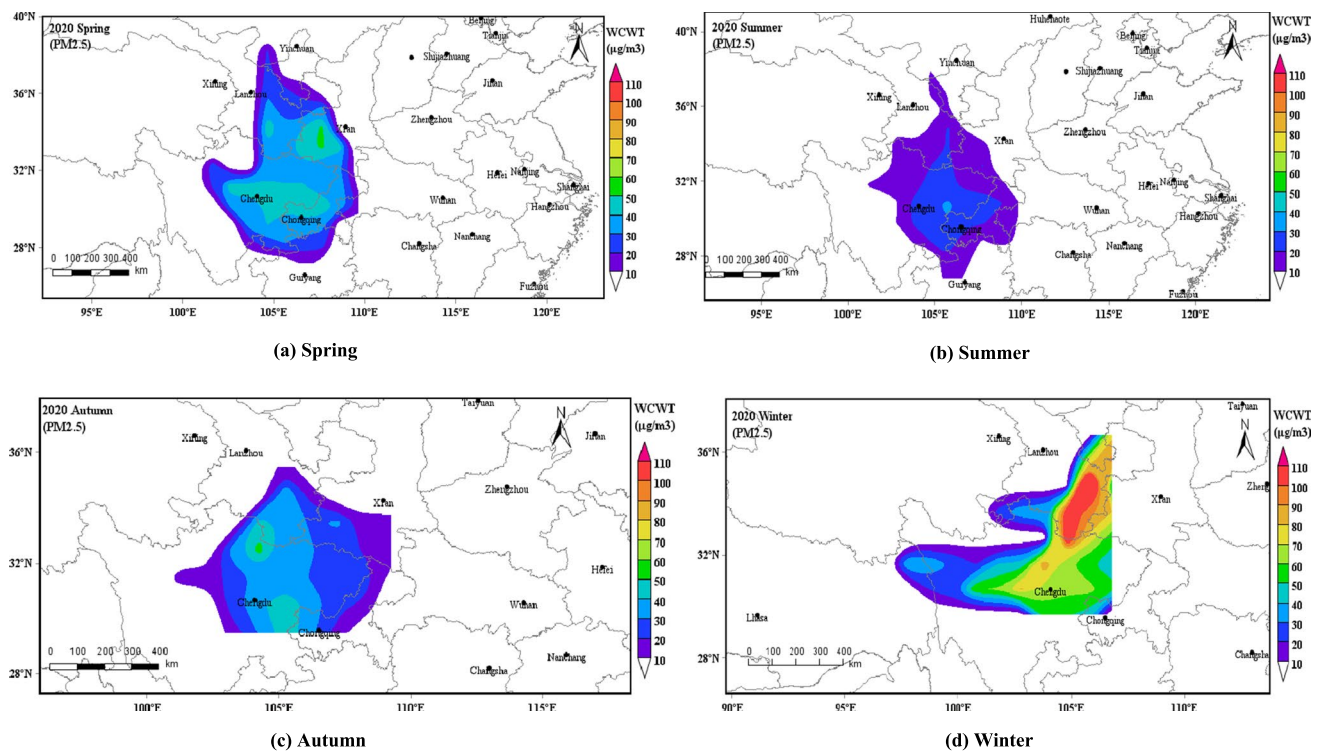


**Fig.18** Spatial distributions of WCWT values for  $PM_{2.5}$  in four seasons of 2020

- (2) Concentrations of pollutants ( $PM_{2.5}$ ,  $PM_{10}$ ,  $NO_2$ ,  $SO_2$ ,  $CO$  and  $NO_2$ ) only showed positive correlation with PRS, and displayed a negatively correlated with other meteorological elements. While,  $O_3$  is only significantly negatively correlated with RHU ( $R = -0.389$ ) and PRS ( $R = -0.894$ ).
- (3) Significant seasonal differences can be observed in the regional transport paths of pollutants ( $PM_{2.5}$  and  $O_3$ ) in 2020. In addition, these pollutants concentration are not only affected by local source emissions, but regional transport (Chongqing, Lhasa, Lanzhou, Xi'an, Guiyang and other cities) is also an important source of contribution. Besides, the high-concentration contribution source areas of  $PM_{2.5}$  and  $O_3$  mainly appear in winter and summer respectively, and the contribution source areas are centralized in Chengdu and its surrounding areas (SCB) and cities.

In general, methods such as kriging interpolation and backward trajectory models, can reflect more specific information on the spatial distribution characteristics of pollutants and potential source areas, and better represent the spatial heterogeneity of pollutants. Therefore, regional pollution prevention and control cannot be a "one-size-fits-all" approach. It requires a detailed analysis of regional distribution characteristics, and dynamic and coordinated emission reduction across the entire region based

on time, area, grade, and category differences to improve the effectiveness of pollution control. Strengthen the management of key industries in the region, screen enterprises with good emission reduction effects and implement refined management and control, focusing on controlling emissions from transportation, construction, industry, etc. In addition, the results of the study show that in autumn and winter, the focus should be on reducing  $PM_{2.5}$  emissions, especially in the central urban area; in summer, more attention should be paid to reducing  $O_3$  pollution in surrounding counties and districts. Accurately quantifying the nonlinear relationship between precursors (such as  $NO_x$ ,  $NH_3$  and VOCs) and  $PM_{2.5}$  and  $O_3$  is the key to achieving coordinated prevention and control of pollutants, which will bring greater environmental and health benefits. Therefore, the main focus should be on the coordinated reduction of  $PM_{2.5}$  and  $O_3$  emissions, detailed analysis of heavy pollution incidents, and promotion of coordinated reduction of multiple pollutants. It also is necessary to continue to study the interaction mechanism of extreme weather, climate change, urbanization and pollutants. At the same time, the effectiveness evaluation of measures and policies is also crucial to improving air quality.

Finally, the impact of pollutant exposure on health should be further quantitatively evaluated to promote the positive health benefits of pollution prevention and control. Local Environment Agency Plans should also be developed as an integrated management plan to assess, prioritize and provide solutions to local environmental issues related to the air pollution and encourage

stakeholders to work together to preserve and protect their local environment.

**Supplementary Information** The online version contains supplementary material available at <https://doi.org/10.1007/s11869-024-01630-2>.

**Acknowledgements** The authors would like to acknowledge to Department of Chemical and Environmental Engineering, Universiti Putra Malaysia and Xichang University, Sichuan Province, China for assistance and helpful with supporting to the writing of this article.

**Funding** This work was supported by the National Natural Science Foundation, China [grant numbers: 41967033]; the Municipal research project of Xichang Sichuan Province, China [grant numbers: 18JSYJ09]; the scientific research project of Xichang University, China [grant numbers: YBZ202125]; and the Project of Sichuan Meteorological Disaster Forecasting, Early Warning and Emergency Management Research Center, Sichuan Province, China [grant numbers: ZHYJ21-YB08].

**Data availability** Data openly available in a public repository.

## Declarations

**Ethics approval** My manuscript does not report on or involve the use of any animal or human data or tissue.

**Consent to participate** Not applicable.

**Consent for publication** Not applicable.

**Competing of interests** The authors declare that they have no known competing financial interests or personal relationships that could have appeared to influence the work reported in this paper.

## References

- Alexeeff SE, Roy A, Shan J, Ray GT, Quesenberry CQ, Apte J, Portier CJ, Van Den Eeden SK (2022) Association between traffic related air pollution exposure and direct health care costs in Northern California. *Atmos Environ* 287:119271. <https://doi.org/10.1016/j.atmosenv.2022.119271>
- Azmi WNF, Pillai TR, Latif MT, Koshy S, Shaharudin R (2023) Application of land use regression model to assess outdoor air pollution exposure: A review. *Environmental Advances* 11:100353. <https://doi.org/10.1016/j.envadv.2023.100353>
- Bai D, Wang H, Cheng M, Gao W, Yang Y, Huang W, Ma K, Zhang Y, Zhang R, Zou J, Wang J, Liang Y, Li N, Wang Y (2021) Source apportionment of PM<sub>2.5</sub> and its optical properties during a regional haze episode over north China plain. *Atmospheric Pollut Res* 12(1):89–99. <https://doi.org/10.1016/j.apr.2020.08.023>
- Bai X, Tian H, Liu X, Wu B, Liu S, Hao Y (2021) Spatial-temporal variation characteristics of air pollution and apportionment of contributions by different sources in Shanxi province of China. *Atmos Environ* 244:117926. <https://doi.org/10.1016/j.atmosenv.2020.117926>
- Bashir MF, Jiang B, Komal B, Bashir MA, Farooq TH, Iqbal N, Bashir M (2020) Correlation between environmental pollution indicators and COVID-19 pandemic: A brief study in Californian context. *Environ Res* 187:109652. <https://doi.org/10.1016/j.envres.2020.109652>
- Beauchamp M, Malherbe L, de Fouquet C, Létinois L, Tognet F (2018) A polynomial approximation of the traffic contributions for kriging-based interpolation of urban air quality model. *Environ Model Softw* 105:132–152. <https://doi.org/10.1016/j.envsoft.2018.03.033>
- Berriban, I., Azahra, M., Chham, E., Ferro-García, M. A., Milena-Pérez, A., Nouayti, A., Orza, J. A. G., Brattich, E., Tositti, L., Piñero-García, F., El Bardouni, T., Ziani, H., El Yaakoubi, H., & El Barbari, M. (2022). PSCF and CWT methods as a tool to identify potential sources of 7Be and 210Pb aerosols in Granada, Spain. *Journal of Environmental Radioactivity*, 251–252. <https://doi.org/10.1016/j.jenvrad.2022.106977>
- Cao Y, Qiao X, Hopke PK, Ying Q, Zhang Y, Zeng Y, Yuan Y, Tang Y (2020) Ozone pollution in the west China rain zone and its adjacent regions, Southwestern China: Concentrations, ecological risk, and Sources. *Chemosphere* 256:127008. <https://doi.org/10.1016/j.chemosphere.2020.127008>
- Cao X, Xing Q, Hu S, Xu W (2023) Characterization, reactivity, source apportionment, and potential source areas of ambient volatile organic compounds in a typical tropical city. *J Environ Sci* 123:417–429. <https://doi.org/10.1016/j.jes.2022.08.005>
- Chen D, Zhou L, Wang C, Liu H, Qiu Y, Shi G, Song D, Tan Q, Yang F (2022) Characteristics of ambient volatile organic compounds during spring O<sub>3</sub> pollution episode in Chengdu, China. *J Environ Sci (China)* 114:115–125. <https://doi.org/10.1016/j.jes.2021.08.014>
- Chen L, Zhang J, Huang X, Li H, Dong G, Wei S (2022) Characteristics and pollution formation mechanism of atmospheric fine particles in the megacity of Chengdu. *China Atmos Res* 273:106172. <https://doi.org/10.1016/j.atmosres.2022.106172>
- Chen Y, Li H, Karimian H, Li M, Fan Q, Xu Z (2022) Spatio-temporal variation of ozone pollution risk and its influencing factors in China based on Geodetector and Geospatial models. *Chemosphere* 302:134843. <https://doi.org/10.1016/j.chemosphere.2022.134843>
- de Foy B, Heo J, Kang JY, Kim H, Schauer JJ (2021) Source attribution of air pollution using a generalized additive model and particle trajectory clusters. *Sci Total Environ* 780:146458. <https://doi.org/10.1016/j.scitotenv.2021.146458>
- Deng Y, Li J, Li Y, Wu R, Xie S (2019) Characteristics of volatile organic compounds, NO<sub>2</sub>, and effects on ozone formation at a site with high ozone level in Chengdu. *J Environ Sci* 75:334–345. <https://doi.org/10.1016/j.jes.2018.05.004>
- Deng J, Zhao W, Wu L, Hu W, Ren L, Wang X, Fu P (2020) Black carbon in Xiamen, China: Temporal variations, transport pathways and impacts of synoptic circulation. *Chemosphere* 241:125133. <https://doi.org/10.1016/j.chemosphere.2019.125133>
- Dimitriou K, Tsagkaraki M, Zarpas P, Mihalopoulos N (2022) Impact of spatial and vertical distribution of air masses on PM<sub>10</sub> chemical components at the Eastern Mediterranean – A seasonal approach. *Atmos Res* 266:105974. <https://doi.org/10.1016/j.atmosres.2021.105974>
- Dong F, Zhu J, Li Y, Chen Y, Gao Y, Hu M, Qin C, Sun J (2022) How green technology innovation affects carbon emission efficiency: evidence from developed countries proposing carbon neutrality targets. *Environ Sci Pollut Res* 29(24):35780–35799. <https://doi.org/10.1007/s11356-022-18581-9>
- Fan J, Shang Y, Zhang X, Wu X, Zhang M (2019) Joint pollution and source apportionment of PM<sub>2.5</sub> among three different urban environments in Sichuan Basin China. *Sci Total Environ* 714:136305. <https://doi.org/10.1016/j.scitotenv.2019.136305>
- Fan H, Zhao C, Yang Y, Yang X (2021) Spatio-Temporal Variations of the PM<sub>2.5</sub>/PM<sub>10</sub> Ratios and Its Application to Air Pollution

- Type Classification in China. *Front Environ Sci* 9:1–13. <https://doi.org/10.3389/fenvs.2021.692440>
- Feng X, Zhang X, Wang J (2023) Update of SO<sub>2</sub> emission inventory in the Megacity of Chongqing China by Inverse Modeling. *Atmos Environ* 294:119519. <https://doi.org/10.1016/j.atmosenv.2022.119519>
- Flores RM, Mertoğlu E, Özdemir H, Akkoyunlu BO, Demir G, Ünal A, Tayanç M (2020) A high-time resolution study of PM<sub>2.5</sub>, organic carbon, and elemental carbon at an urban traffic site in Istanbul. *Atmos Environ* 223:1–9. <https://doi.org/10.1016/j.atmosenv.2019.117241>
- Gao X, Xiao J, Qin H, Cao Z, Wang H (2016) Impact of meteorological factors on the prevalence of porcine pasteurellosis in the southcentral of Mainland China. *Prev Vet Med* 125:75–81. <https://doi.org/10.1016/j.pvetmed.2016.01.002>
- Gao C, Zhang F, Fang D, Wang Q, Liu M (2023) Spatial characteristics of change trends of air pollutants in Chinese urban areas during 2016–2020: The impact of air pollution controls and the COVID-19 pandemic. *Atmos Res* 283:106539. <https://doi.org/10.1016/j.atmosres.2022.106539>
- Gogikar P, Tyagi B (2016) Assessment of particulate matter variation during 2011–2015 over a tropical station Agra, India. *Atmos Environ* 147:11–21. <https://doi.org/10.1016/j.atmosenv.2016.09.063>
- Gómez González L, Linares C, Díaz J, Egea A, Calle-Martínez A, Luna MY, Navas MA, Ascaso-Sánchez MS, Ruiz-Páez R, Asensio C, Padrón-Monedero A, López-Bueno JA (2023) Short-term impact of noise, other air pollutants and meteorological factors on emergency hospital mental health admissions in the Madrid region. *Environ Res* 224:115505. <https://doi.org/10.1016/j.envres.2023.115505>
- Gonzalez JN, Gomez J, Vassallo JM (2022) Do urban parking restrictions and Low Emission Zones encourage a greener mobility? *Transp Res Part d: Transp Environ* 107:103319. <https://doi.org/10.1016/j.trd.2022.103319>
- Hou X, Guo Q, Hong Y, Yang Q, Wang X, Zhou S, Liu H (2022) Assessment of PM<sub>2.5</sub>-related health effects: A comparative study using multiple methods and multi-source data in China. *Environ Pollut* 306:119381. <https://doi.org/10.1016/j.envpol.2022.119381>
- Hu Y, Wang S (2021) Formation mechanism of a severe air pollution event: A case study in the Sichuan Basin. *Southwest China Atmos Environ* 246:118135. <https://doi.org/10.1016/j.atmosenv.2020.118135>
- Huang W, Long E, Wang J, Huang R, Ma L (2015) Characterizing spatial distribution and temporal variation of PM<sub>10</sub> and PM<sub>2.5</sub> mass concentrations in an urban area of Southwest China. *Atmos Pollut Res* 6(5):842–848. <https://doi.org/10.5094/APR.2015.093>
- Jia R, Luo M, Liu Y, Zhu Q, Hua S, Wu C, Shao T (2019) Anthropogenic Aerosol Pollution over the Eastern Slope of the Tibetan Plateau. *Adv Atmos Sci* 36(8):847–862. <https://doi.org/10.1007/s00376-019-8212-0>
- Kaskaoutis DG, Dumka UC, Rashki A, Psiloglou BE, Gavriil A, Mofidi A, Petrinoli K, Karagiannis D, Kambezidis HD (2019) Analysis of intense dust storms over the eastern Mediterranean in March 2018: Impact on radiative forcing and Athens air quality. *Atmos Environ* 209:23–39. <https://doi.org/10.1016/j.atmosenv.2019.04.025>
- Kong L, Tan Q, Feng M, Qu Y, An J, Liu X, Cheng N, Deng Y, Zhai R, Wang Z (2020) Investigating the characteristics and source analyses of PM<sub>2.5</sub> seasonal variations in Chengdu Southwest China. *Chemosphere* 243:125267. <https://doi.org/10.1016/j.chemosphere.2019.125267>
- Konstantinoudis G, Padellini T, Bennett J, Davies B, Ezzati M, Blangiardo M (2021) Long-term exposure to air-pollution and COVID-19 mortality in England : A hierarchical spatial analysis. *Environ Int* 146:106316. <https://doi.org/10.1016/j.envint.2020.106316>
- Kumar A, Kumar R, Sarma K (2020) Mapping spatial distribution of traffic induced criteria pollutants and associated health risks using kriging interpolation tool in Delhi. *J Transp Health* 18:100879. <https://doi.org/10.1016/j.jth.2020.100879>
- Kumar A, Dhakhwa S, Dikshit AK (2022) Comparative Evaluation of Fitness of Interpolation Techniques of ArcGIS Using Leave-One-Out Scheme for Air Quality Mapping. *J Geovisualization Spatial Anal* 6(1):1–11. <https://doi.org/10.1007/s41651-022-00102-4>
- Li D, Liu J, Zhang J, Gui H, Du P, Yu T, Wang J, Lu Y, Liu W, Cheng Y (2017) Identification of long-range transport pathways and potential sources of PM<sub>2.5</sub> and PM<sub>10</sub> in Beijing from 2014 to 2015. *J Environ Sci (china)* 56:214–229. <https://doi.org/10.1016/j.jes.2016.06.035>
- Li L, Tan Q, Zhang Y, Feng M, Qu Y, An J, Liu X (2017) Characteristics and source apportionment of PM<sub>2.5</sub> during persistent extreme haze events in Chengdu, southwest China. *Environ Pollut* 230:718–729. <https://doi.org/10.1016/j.envpol.2017.07.029>
- Li R, Fu H, Cui L, Li J, Wu Y, Meng Y, Wang Y, Chen J (2019) The spatiotemporal variation and key factors of SO<sub>2</sub> in 336 cities across China. *J Clean Prod* 210:602–611. <https://doi.org/10.1016/j.jclepro.2018.11.062>
- Li Y, Xue Y, Guang J, de Leeuw G, Self R, She L, Fan C, Xie Y, Chen G (2019) Spatial and temporal distribution characteristics of haze days and associated factors in China from 1973 to 2017. *Atmos Environ* 214:116862. <https://doi.org/10.1016/j.atmosenv.2019.116862>
- Li Y, An X, Zhang P, Yang J, Wang C, Li J (2021) Influence of East Asian winter monsoon on particulate matter pollution in typical regions of China. *Atmos Environ* 260:118213. <https://doi.org/10.1016/j.atmosenv.2021.118213>
- Li D, Ji A, Lin Z, Liu J, Tan C, Huang X, Xiao H, Tang E, Liu X, Yao C, Li Y, Zhou L, Cai T (2022) Short-term ambient air pollution exposure and adult primary insomnia outpatient visits in Chongqing, China: A time-series analysis. *Environ Res* 212:113188. <https://doi.org/10.1016/j.envres.2022.113188>
- Li J, He Q, Ge X, Abbas A (2022) Spatiotemporal distribution of aerosols over the Tibet Plateau and Tarim Basin (1980–2020). *J Clean Prod* 374:133958. <https://doi.org/10.1016/j.jclepro.2022.133958>
- Li D, Wu Q, Feng J, Wang Y, Wang L, Xu Q, Sun Y, Cao K, Cheng H (2023) The influence of anthropogenic emissions on air quality in Beijing-Tianjin-Hebei of China around 2050 under the future climate scenario. *J Clean Prod* 388:135927. <https://doi.org/10.1016/j.jclepro.2023.135927>
- Liang Z, Xu C, Liang S, Cai TJ, Yang N, Li S, Di, Wang WT, Li YF, Wang D, Ji AL, Zhou LX, Liang ZQ (2021) Short-term ambient nitrogen dioxide exposure is associated with increased risk of spontaneous abortion: A hospital-based study. *Ecotoxicol Environ Safety* 224:112633. <https://doi.org/10.1016/j.ecoenv.2021.112633>
- Liang S, Gao S, Wang S, Chai W, Chen W, Tang G (2023) Characteristics, sources of volatile organic compounds, and their contributions to secondary air pollution during different periods in Beijing. *China Science of the Total Environment* 858:159831. <https://doi.org/10.1016/j.scitotenv.2022.159831>
- Liang Y, Gui K, Che H, Li L, Zheng Y, Zhang X, Zhang X, Zhang P, Zhang X (2023) Changes in aerosol loading before, during and after the COVID-19 pandemic outbreak in China: Effects of anthropogenic and natural aerosol. *Sci Total Environ* 857:159435. <https://doi.org/10.1016/j.scitotenv.2022.159435>

- Liu Z, Gao W, Yu Y, Hu B, Xin J, Sun Y, Wang L, Wang G, Bi X, Zhang G, Xu H, Cong Z, He J, Xu J, Wang Y (2018) Characteristics of PM<sub>2.5</sub> mass concentrations and chemical species in urban and background areas of China: Emerging results from the CARE-China network. *Atmos Chem Phys* 18:8849–8871. <https://doi.org/10.5194/acp-18-8849-2018>
- Liu J, Zheng Y, Geng G, Hong C, Li M, Li X, Liu F, Tong D, Wu R, Zheng B, He K, Zhang Q (2020) Decadal changes in anthropogenic source contribution of PM<sub>2.5</sub> pollution and related health impacts in China, 1990–2015. *Atmos Chem Phys* 20(13):7783–7799. <https://doi.org/10.5194/acp-20-7783-2020>
- Liu T, Hu B, Yang Y, Li M, Hong Y, Xu X, Xu L, Chen N, Chen Y, Xiao H, Chen J (2020) Characteristics and source apportionment of PM<sub>2.5</sub> on an island in Southeast China: Impact of sea-salt and monsoon. *Atmos Res* 235:104786. <https://doi.org/10.1016/j.atmosres.2019.104786>
- Liu S, He N, Shi Y, Li G (2021) The roles logistics agglomeration and technological progress play in air pollution — New evidence in sub-regions of Chongqing China. *J Clean Prod* 317:128414. <https://doi.org/10.1016/j.jclepro.2021.128414>
- Liu H, Liu J, Li M, Gou P, Cheng Y (2022) Assessing the evolution of PM<sub>2.5</sub> and related health impacts resulting from air quality policies in China. *Environ Impact Assess Rev* 93:106727. <https://doi.org/10.1016/j.eiar.2021.106727>
- Liu W, Cai M, Long Z, Tong X, Li Y, Wang L, Zhou M, Wei J, Lin H, Yin P (2023) Association between ambient sulfur dioxide pollution and asthma mortality: Evidence from a nationwide analysis in China. *Ecotoxicol Environ Saf* 249:114442. <https://doi.org/10.1016/j.ecoenv.2022.114442>
- Lotfata A (2022) Using Geographically Weighted Models to Explore Obesity Prevalence Association with Air Temperature, Socio-economic Factors, and Unhealthy Behavior in the USA. *J Geovisualization Spatial Anal* 6(1):1–12. <https://doi.org/10.1007/s41651-022-00108-y>
- Lu H, Xie M, Liu B, Liu X, Feng J, Yang F, Zhao X, You T, Wu Z, Gao Y (2022) Impact of atmospheric thermodynamic structures and aerosol radiation feedback on winter regional persistent heavy particulate pollution in the Sichuan-Chongqing region China. *Sci Total Environ* 842:156575. <https://doi.org/10.1016/j.scitotenv.2022.156575>
- Lu H, Xie M, Liu X, Liu B, Liu C, Zhao X, Du Q, Wu Z, Gao Y, Xu L (2022) Spatial-temporal characteristics of particulate matters and different formation mechanisms of four typical haze cases in a mountain city. *Atmos Environ* 269:118868. <https://doi.org/10.1016/j.atmosenv.2021.118868>
- Luo J, Zhang J, Huang X, Liu Q, Luo B, Zhang W, Rao Z, Yu Y (2020) Characteristics, evolution, and regional differences of biomass burning particles in the Sichuan Basin, China. *J Environ Sci* 89:35–46. <https://doi.org/10.1016/j.jes.2019.09.015>
- Ma W, Ding J, Wang R, Wang J (2022) Drivers of PM<sub>2.5</sub> in the urban agglomeration on the northern slope of the Tianshan Mountains China. *Environ Pollut* 309:119777. <https://doi.org/10.1016/j.envpol.2022.119777>
- Mostafa MK, Gamal G, Wafiq A (2021) The impact of COVID 19 on air pollution levels and other environmental indicators - A case study of Egypt. *J Environ Manage* 277:111496. <https://doi.org/10.1016/j.jenvman.2020.111496>
- National Bureau of Statistics (2022) China Statistical Yearbook[J]. Beijing: China Statistics Press. <https://www.stats.gov.cn/sj/ndsj/2022/indexch.htm>
- Ning G, Yim SHL, Wang S, Duan B, Nie C, Yang X, Wang J, Shang K (2019) Synergistic effects of synoptic weather patterns and topography on air quality: a case of the Sichuan Basin of China. *Clim Dyn* 53(11):6729–6744. <https://doi.org/10.1007/s00382-019-04954-3>
- Peng X, Huang XF, Wei FH, Yan RH, Tang MX, Ji JP, He LY (2022) Identifying the key drivers in retrieving blue sky during rapid urbanization in Shenzhen China. *J Clean Prod* 356(April):131829. <https://doi.org/10.1016/j.jclepro.2022.131829>
- Pinto JA, Kumar P, Alonso MF, Andreão WL, Pedruzzi R, Espinosa SI, de Almeida Albuquerque TT (2020) Kriging method application and traffic behavior profiles from local radar network database: A proposal to support traffic solutions and air pollution control strategies. *Sustain Cities Soc* 56:102062. <https://doi.org/10.1016/j.scs.2020.102062>
- Qi N, Tan X, Wu T, Tang Q, Ning F, Jiang D, Xu T, Wu H (2022) Temporal and Spatial Distribution Analysis of Atmospheric Pollutants in Chengdu – Chongqing Twin-City Economic Circle. *Int J Environ Res Publ Health* 19(7):4333
- Qi G, Che J, Wang Z (2023) Differential effects of urbanization on air pollution: Evidences from six air pollutants in mainland China. *Ecol Ind* 146(2):109924. <https://doi.org/10.1016/j.ecolind.2023.109924>
- Qiao X, Liu L, Yang C, Yuan Y, Zhang M, Guo H, Tang Y, Ying Q, Zhu S, Zhang H (2021) Responses of fine particulate matter and ozone to local emission reductions in the Sichuan Basin, southwestern China. *Environ Pollut* 277:116793. <https://doi.org/10.1016/j.envpol.2021.116793>
- Romshoo SA, Bhat MA, Beig G (2021) Particulate pollution over an urban Himalayan site: Temporal variability, impact of meteorology and potential source regions. *Sci Total Environ* 799:149364. <https://doi.org/10.1016/j.scitotenv.2021.149364>
- Sasmitha S, Kumar DB, Priyadharshini B (2022) Assessment of sources and health impacts of PM<sub>10</sub> in an urban environment over eastern coastal plain of India. *Environ Chall* 7:100457. <https://doi.org/10.1016/j.envc.2022.100457>
- Sen, A., Abdelmaksoud, A. S., Nazeer Ahammed, Y., Alghamdi, M. ., Banerjee, T., Bhat, M. A., Chatterjee, A., Choudhuri, A. K., Das, T., Dhir, A., Dhyani, P. P., Gadi, R., Ghosh, S., Kumar, K., Khan, A. H., Khoder, M., Maharaj Kumari, K., Kuniyal, J. C., Kumar, M., ... Mandal, T. K. (2017). Variations in particulate matter over Indo-Gangetic Plains and Indo-Himalayan Range during four field campaigns in winter monsoon and summer monsoon: Role of pollution pathways. *Atmospheric Environment*, 154, 200–224. <https://doi.org/10.1016/j.atmosenv.2016.12.054>
- Shukla K, Kumar P, Mann GS, Khare M (2020) Mapping spatial distribution of particulate matter using Kriging and Inverse Distance Weighting at supersites of megacity Delhi. *Sustain Cities Soc* 54:101997. <https://doi.org/10.1016/j.scs.2019.101997>
- Song S, Li T, Liu P, Li Z (2022) The transition pathway of energy supply systems towards carbon neutrality based on a multi-regional energy infrastructure planning approach: A case study of China. *Energy* 238:122037. <https://doi.org/10.1016/j.energy.2021.122037>
- Song T, Feng M, Song D, Zhou L, Qiu Y, Tan Q, Yang F (2022) Enhanced nitrate contribution during winter haze events in a megacity of Sichuan Basin, China: Formation mechanism and source apportionment. *J Clean Prod* 370(February):133272. <https://doi.org/10.1016/j.jclepro.2022.133272>
- Tan S, Xie D, Ni C, Zhao G, Shao J, Chen F, Ni J (2023) Spatiotemporal characteristics of air pollution in Chengdu-Chongqing urban agglomeration (CCUA) in Southwest, China: 2015–2021. *J Environ Manag* 325:116503. <https://doi.org/10.1016/j.jenvman.2022.116503>
- Tarasov DA, Buevich AG, Sergeev AP, Shichkin AV (2018) High variation topsoil pollution forecasting in the Russian Subarctic: Using artificial neural networks combined with residual kriging.

- Appl Geochem 88:188–197. <https://doi.org/10.1016/j.apgeochem.2017.07.007>
- Tian X, Ren B, Xie P, Xu J, Li A, Hu F, Zheng J, Ren H (2022) The vertical distribution and potential sources of aerosols in the Yangtze River Delta region of China during open straw burning. *Sci Total Environ* 849(January):157749. <https://doi.org/10.1016/j.scitotenv.2022.157749>
- Wang H, Yang F, Shi G, Tian M, Zhang L, Zhang L, Fu C (2016) Ambient concentration and dry deposition of major inorganic nitrogen species at two urban sites in Sichuan Basin, China. *Environ Pollut* 219:235–244. <https://doi.org/10.1016/j.envpol.2016.10.016>
- Wang H, Qiao B, Zhang L, Yang F, Jiang X (2018) Characteristics and sources of trace elements in PM 2.5 in two megacities in Sichuan Basin of southwest China. *Environ Pollut* 242:1577–1586. <https://doi.org/10.1016/j.envpol.2018.07.125>
- Wang W, Yu J, Cui Y, He J, Xue P, Cao W, Ying H, Gao W, Yan Y, Hu B, Xin J, Wang L, Liu Z, Sun Y, Ji D, Wang Y (2018) Characteristics of fine particulate matter and its sources in an industrialized coastal city, Ningbo, Yangtze River Delta, China. *Atmos Res* 203:105–117. <https://doi.org/10.1016/j.atmosres.2017.11.033>
- Wang X, Chen L, Guo K, Liu B (2022) Spatio-temporal trajectory evolution and cause analysis of air pollution in Chengdu, China. *J Air Waste Manag Assoc* 72(8):876–894. <https://doi.org/10.1080/10962247.2022.2058642>
- Wang J, Li J, Li X, Fang C (2022) Characteristics of Air Pollutants Emission and Its Impacts on Public Health of Chengdu, Western China. *Int J Environ Res Public Health* 19:16852. <https://doi.org/10.3390/ijerph192416852>
- Xia X, Zhang K, Yang R, Zhang Y, Xu D, Bai K, Guo J (2022) Impact of near-surface turbulence on PM2.5 concentration in Chengdu during the COVID-19 pandemic. *Atmos Environ* 268:118848. <https://doi.org/10.1016/j.atmosenv.2021.118848>
- Xu H, Zeng W, Guo B, Hopke PK, Qiao X, Choi H, Luo B, Zhang W, Zhao X (2020) Improved risk communications with a Bayesian multipollutant Air Quality Health Index. *Sci Total Environ* 722:137892. <https://doi.org/10.1016/j.scitotenv.2020.137892>
- Xu H, Liu S, Wang Y, Wu R, Yi T, Wang T, Zhu Y, Fang J, Xie Y, Zhao Q, Song X, Chen J, Rajagopalan S, Brook RD, Li J, Cao J, Huang W (2022) The mediating role of vascular inflammation in traffic-related air pollution associated changes in insulin resistance in healthy adults. *Int J Hygiene Environ Health* 239:113878. <https://doi.org/10.1016/j.ijheh.2021.113878>
- Xu T, Zhang C, Liu C, Hu Q (2023) Variability of PM2.5 and O3 concentrations and their driving forces over Chinese megacities during 2018–2020. *J Environ Sci* 124:1–10. <https://doi.org/10.1016/j.jes.2021.10.014>
- Xu H, Liu Y, Wang Q, Ma R, Ban J, Li T (2024) The disease burden related to time-weighted PM2.5 exposure in China and the potential health benefits of the national standards for indoor air quality: A modeling study. *Sustain Horizons* 9:100078. <https://doi.org/10.1016/j.horiz.2023.100078>
- Yang J, Hu M (2018) Science of the Total Environment Filling the missing data gaps of daily MODIS AOD using spatiotemporal interpolation. *Sci Total Environ* 633:677–683. <https://doi.org/10.1016/j.scitotenv.2018.03.202>
- Yang J, Ji Z, Kang S, Zhang Q, Chen X, Lee S (2019) Spatiotemporal variations of air pollutants in western China and their relationship to meteorological factors and emission sources \*. *Environ Pollut* 254:112952. <https://doi.org/10.1016/j.envpol.2019.07.120>
- Yang J, Kang S, Chen D, Ji Z, Tripathee L, Chen X, Du W, Qiu G (2019) Quantifying the contributions of various emission sources to black carbon and assessment of control strategies in western China. *Atmos Res* 215:178–192. <https://doi.org/10.1016/j.atmosres.2018.09.003>
- Yang X, Wu K, Wang H, Liu Y, Gu S, Lu Y, Zhang X, Hu Y, Ou Y, Wang S, Wang Z (2020) Summertime ozone pollution in Sichuan Basin, China: Meteorological conditions, sources and process analysis. *Atmos Environ* 226:117392. <https://doi.org/10.1016/j.atmosenv.2020.117392>
- Yu H, Yang W, Wang X, Yin B, Zhang X, Wang J, Gu C, Ming J, Geng C, Bai Z (2019) A seriously sand storm mixed air-polluted area in the margin of Tarim Basin: Temporal-spatial distribution and potential sources. *Sci Total Environ* 676:436–446. <https://doi.org/10.1016/j.scitotenv.2019.04.298>
- Zhan CC, Xie M, Fang DX, Wang TJ, Wu Z, Lu H, Zhao M (2019) Synoptic weather patterns and their impacts on regional particle pollution in the city cluster of the Sichuan Basin, China. *Atmos Environ* 208:34–47. <https://doi.org/10.1016/j.atmosenv.2019.03.033>
- Zhang H, Wang Y, Hu J, Ying Q, Hu XM (2015) Relationships between meteorological parameters and criteria air pollutants in three megacities in China. *Environ Res* 140:242–254. <https://doi.org/10.1016/j.envres.2015.04.004>
- Zhang Y, Cai J, Wang S, He K, Zheng M (2017) Review of receptor-based source apportionment research of fine particulate matter and its challenges in China. *Sci Total Environ* 586:917–929. <https://doi.org/10.1016/j.scitotenv.2017.02.071>
- Zhang NN, Ma F, Qin CB, Li YF (2018) Spatiotemporal trends in PM2.5 levels from 2013 to 2017 and regional demarcations for joint prevention and control of atmospheric pollution in China. *Chemosphere* 210:1176–1184. <https://doi.org/10.1016/j.chemosphere.2018.07.142>
- Zhang S, An K, Li J, Weng Y, Zhang S, Wang S, Cai W, Wang C, Gong P (2021) Incorporating health co-benefits into technology pathways to achieve China's 2060 carbon neutrality goal: a modelling study. *Lancet Planet Health* 5(11):e808–e817. [https://doi.org/10.1016/S2542-5196\(21\)00252-7](https://doi.org/10.1016/S2542-5196(21)00252-7)
- Zhang X, Tang M, Guo F, Wei F, Yu Z, Gao K, Jin M, Wang J, Chen K (2021) Associations between air pollution and COVID-19 epidemic during quarantine period in China. *Environ Pollut* 268:115897. <https://doi.org/10.1016/j.envpol.2020.115897>
- Zhang B, Wang S, Wang D, Wang Q, Yang X, Tong R (2022) Air quality changes in China 2013–2020: Effectiveness of clean coal technology policies. *J Clean Prod* 366:132961. <https://doi.org/10.1016/j.jclepro.2022.132961>
- Zhang J, Li H, Chen L, Huang X, Zhang W, Zhao R (2022) Particle composition, sources and evolution during the COVID-19 lockdown period in Chengdu, southwest China: Insights from single particle aerosol mass spectrometer data. *Atmos Environ* 268:118844. <https://doi.org/10.1016/j.atmosenv.2021.118844>
- Zhang S, Zhang R, Guo D, Han Y, Song G, Yang F, Chen Y (2022) Molecular mechanism of Pulmonary diseases caused by exposure to urban PM2.5 in Chengdu-Chongqing Economic Circle China. *Environ Int* 165:107292. <https://doi.org/10.1016/j.envint.2022.107292>
- Zhang Z, Zhu W, Hu M, Wang H, Tang L, Hu S, Shen R, Yu Y, Song K, Tan R, Chen Z, Chen S, Canonaco F, Prévôt ASH, Guo S (2023) Secondary organic aerosol formation in China from urban-lifestyle sources: Vehicle exhaust and cooking emission. *Sci Total Environ* 857:159340. <https://doi.org/10.1016/j.scitotenv.2022.159340>
- Zhou Z, Tan Q, Deng Y, Lu C, Song D, Zhou X, Zhang X, Jiang X (2021) Source profiles and reactivity of volatile organic compounds from anthropogenic sources of a megacity in southwest China. *Sci Total Environ* 790:148149. <https://doi.org/10.1016/j.scitotenv.2021.148149>
- Zhou X, Gao X, Chang Y, Zhao S, Li P (2023) The pattern and mechanism of an unhealthy air pollution event in Lanzhou China. *Urban Clim* 48:101409. <https://doi.org/10.1016/j.uclim.2023.101409>

- Zhu Y, Zhan Y, Wang B, Li Z, Qin Y, Zhang K (2019) Spatiotemporally mapping of the relationship between NO<sub>2</sub> pollution and urbanization for a megacity in Southwest China during 2005–2016. *Chemosphere* 220(2):155–162. <https://doi.org/10.1016/j.chemosphere.2018.12.095>
- Zhu Y, Wang Y, Xu H, Luo B, Zhang W, Guo B, Chen S, Zhao X, Li W (2020) Joint effect of multiple air pollutants on daily emergency department visits in Chengdu China. *Environ Pollut* 257:113548. <https://doi.org/10.1016/j.envpol.2019.113548>

**Publisher's Note** Springer Nature remains neutral with regard to jurisdictional claims in published maps and institutional affiliations.

Springer Nature or its licensor (e.g. a society or other partner) holds exclusive rights to this article under a publishing agreement with the author(s) or other rightsholder(s); author self-archiving of the accepted manuscript version of this article is solely governed by the terms of such publishing agreement and applicable law.